

# Numerical methods for studying the behavior of low-dimensional nonlinear dynamical systems

Haris Skokos

Nonlinear Dynamics and Chaos (NDC) group  
Department of Mathematics and Applied Mathematics  
University of Cape Town, South Africa

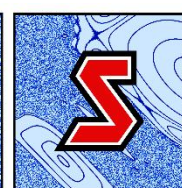
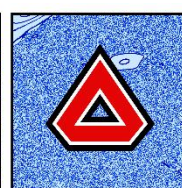
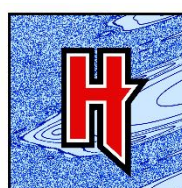
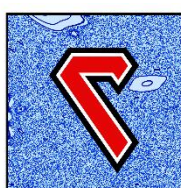
&

Max Planck Institute for the Physics of Complex Systems  
Dresden, Germany

E-mail: [haris.skokos@uct.ac.za](mailto:haris.skokos@uct.ac.za), [haris.skokos@gmail.com](mailto:haris.skokos@gmail.com)  
URL: [http://math\\_research.uct.ac.za/~hskokos/](http://math_research.uct.ac.za/~hskokos/)

Centre de Physique Théorique (CPT), Marseille, France

4 December 2025



MAX-PLANCK-INSTITUT  
FÜR PHYSIK KOMPLEXER SYSTEME

# Outline

- Lagrangian descriptors (LDs)
- Smaller Alignment Index (SALI)
- Chaos diagnostics based on LDs:
  - ✓ the difference of LDs of neighboring orbits
  - ✓ the ratio of LDs of neighboring orbits
  - ✓ a quantity related to the finite-difference second spatial derivative of LDs
  - ✓ Applications: Hénon – Heiles system, 2D Standard map, 4D Standard map
- The origin fate map (OFM)
  - ✓ The 2 degree of freedom caldera Hamiltonian system
  - ✓ Definition of the OFM
  - ✓ Visualization of phase space transport
  - ✓ Relation to the morphology of manifolds
  - ✓ Locating the position of unstable periodic orbits
- Summary

# Lagrangian descriptors (LDs)

The computation of LDs is based on the accumulation of some positive scalar value along the path of individual orbits.

Consider an  $N$  dimensional continuous time dynamical system

$$\dot{x} = \frac{dx(t)}{dt} = f(x, t)$$

**The arclength definition** (Madrid, Mancho, Chaos, 2009 – Mendoza, Mancho, PRL, 2010 – Mancho et al., Commun. Nonlin. Sci. Num. Simul., 2013).

**Forward time  $LD$ :**

$$LD^f(x, \tau) = \int_0^\tau \|\dot{x}(t)\| dt$$

**Backward time  $LD$ :**

$$LD^b(x, \tau) = \int_{-\tau}^0 \|\dot{x}(t)\| dt$$

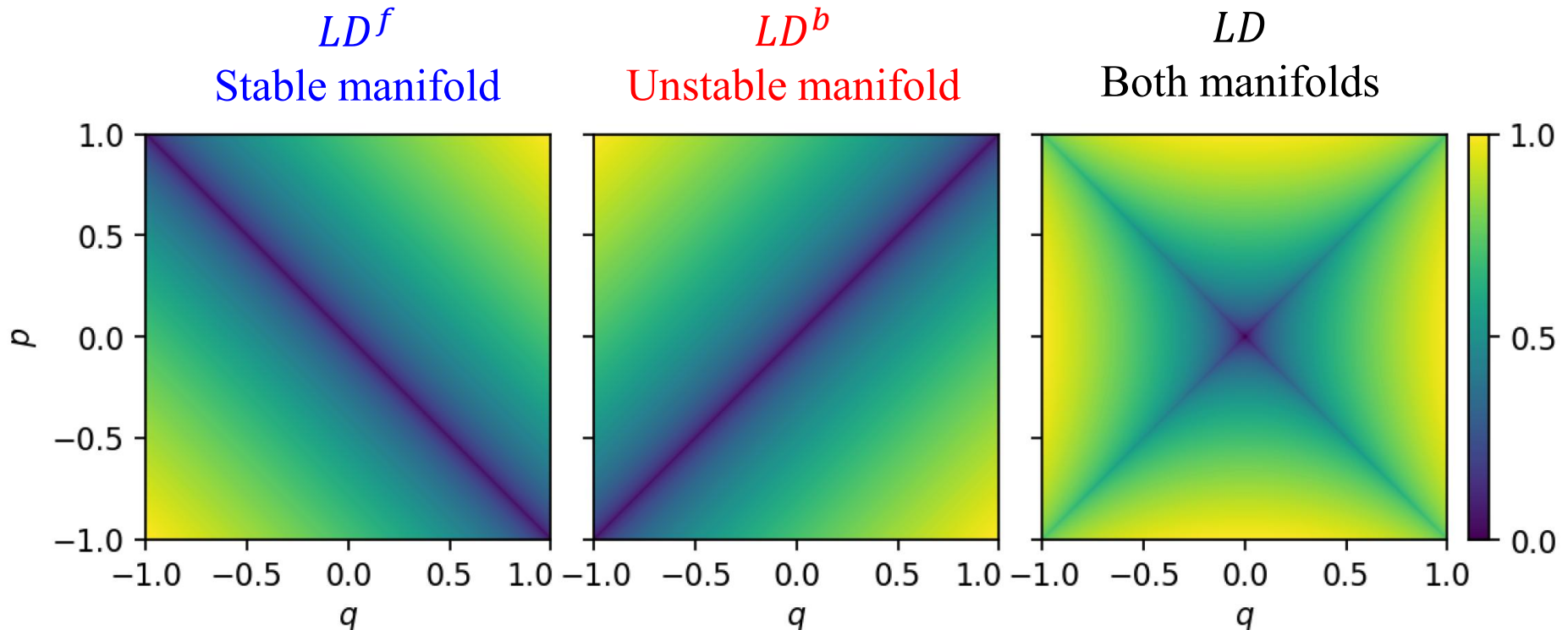
**Combined  $LD$ :**

$$LD(x, \tau) = LD^b(x, \tau) + LD^f(x, \tau)$$

# LDs: 1 degree of freedom (dof) Hamiltonian

$$H(q, p) = \frac{1}{2} (p^2 - q^2)$$

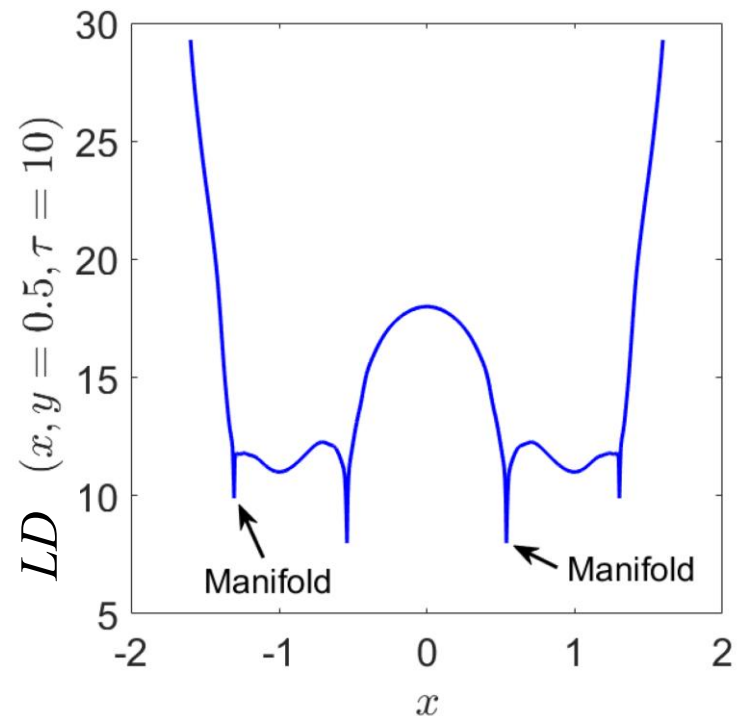
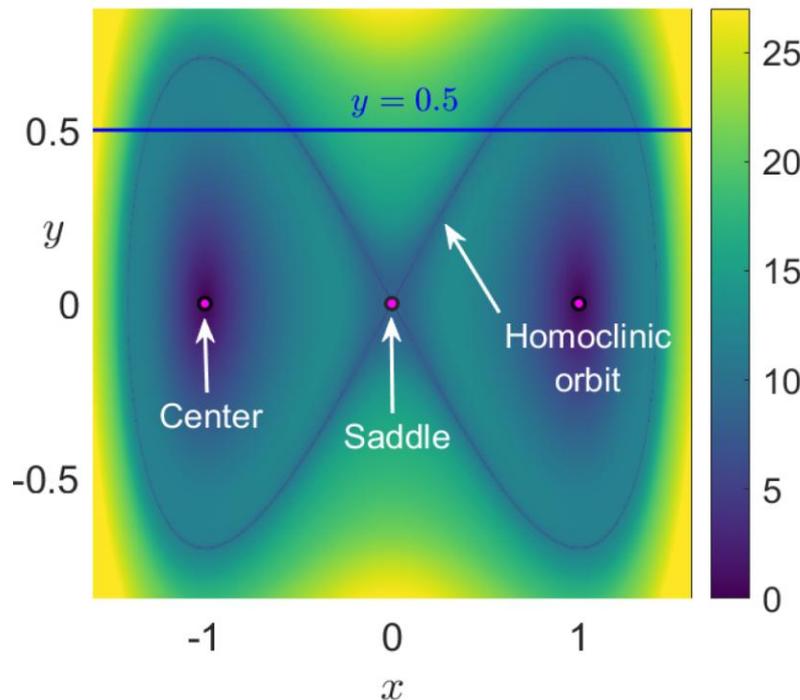
The system has a hyperbolic fixed point at the origin. The LDs can be used to display the stable and unstable manifolds of this point.



# LDs: 1 dof Duffing Oscillator

$$H(x, y) = \frac{1}{2}y^2 + \frac{1}{4}x^4 - \frac{1}{2}x^2$$

The system has three equilibrium points: a saddle located at the origin and two diametrically opposed centers at the points  $(\pm 1, 0)$ .



From Agaoglou et al. 'Lagrangian descriptors: Discovery and quantification of phase space structure and transport', 2020, <https://doi.org/10.5281/zenodo.3958985>

The **location of the stable and unstable manifolds** can be extracted from the ridges of the **gradient field of the LDs** since they are located at **points where the forward and the backward components of the LD are non-differentiable**.

# Lagrangian descriptors (LDs)

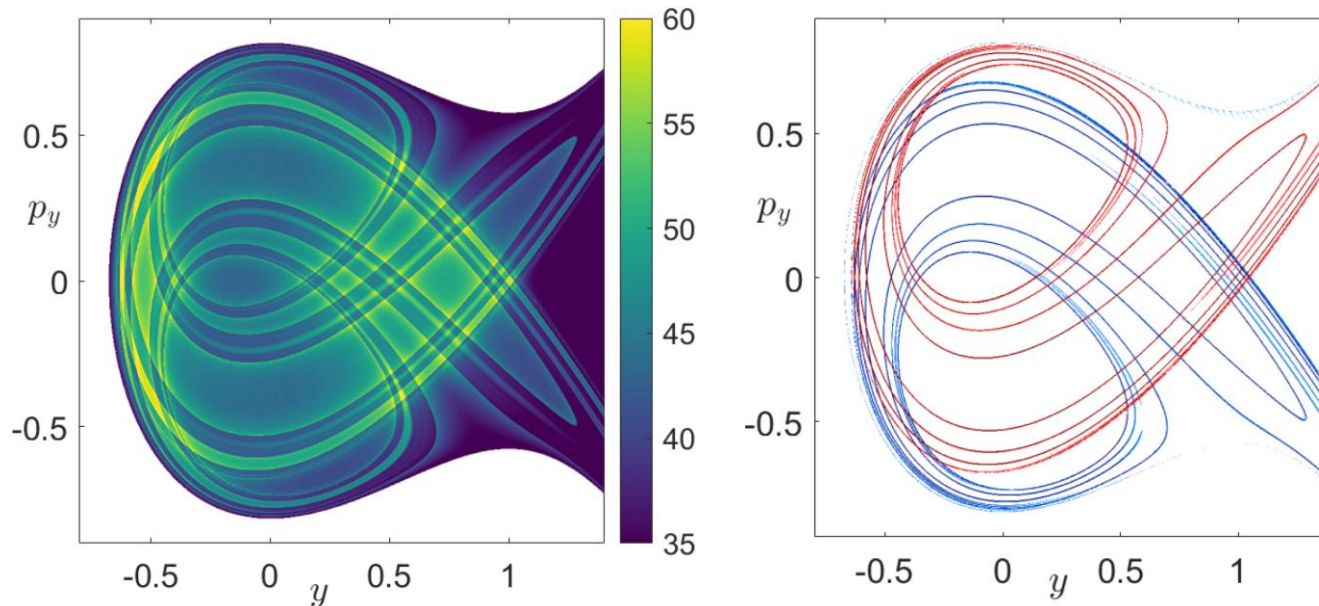
The '*p*-norm' definition (Lopesino et al., Commun. Nonlin. Sci. Num. Simul., 2015 – Lopesino et al., Int. J. Bifurcat. Chaos, 2017).

Combined *LD* (usually  $p=1/2$ ):

$$LD(x, \tau) = \int_{-\tau}^{\tau} \left( \sum_{i=1}^N |f_i(x, t)|^p \right) dt$$

Hénon-Heiles system:  $H = \frac{1}{2} (p_x^2 + p_y^2) + \frac{1}{2} (x^2 + y^2) + x^2 y - \frac{1}{3} y^3$

Stable and unstable manifolds for  $H=1/3$ ,  $\tau=10$ .



# Maximum Lyapunov Exponent (MLE)

Chaos: sensitive dependence on initial conditions.

Roughly speaking, the MLE of a given orbit characterizes the **mean exponential rate of divergence** of trajectories surrounding it.

Consider an orbit in the  $2N$ -dimensional phase space with **initial condition  $x(0)$**  and **an initial deviation vector (small perturbation) from it  $v(0)$** .

Then the mean exponential rate of divergence is:

$$MLE = \lambda_1 = \lim_{t \rightarrow \infty} \Lambda(t) = \lim_{t \rightarrow \infty} \frac{1}{t} \ln \frac{\|v(t)\|}{\|v(0)\|}$$

$\lambda_1 = 0 \rightarrow$  Regular motion ( $\Lambda \propto t^{-1}$ )

$\lambda_1 > 0 \rightarrow$  Chaotic motion

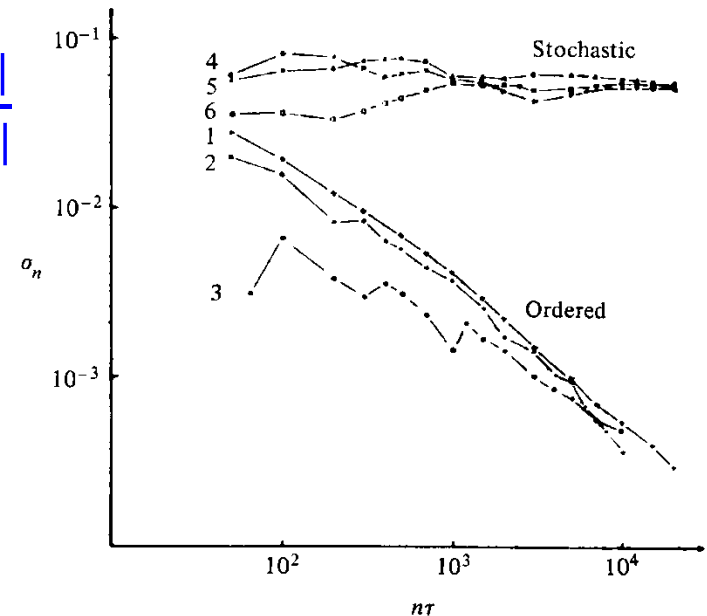


Figure 5.7. Behavior of  $\sigma_n$  at the intermediate energy  $E = 0.125$  for initial points taken in the ordered (curves 1-3) or stochastic (curves 4-6) regions (after Benettin *et al.*, 1976).

# The Smaller Alignment Index (SALI)

Consider the  $2N$ -dimensional phase space of a conservative dynamical system (symplectic map or Hamiltonian flow).

An orbit in that space with initial condition :

$$P(0) = (x_1(0), x_2(0), \dots, x_{2N}(0))$$

and a deviation vector

$$v(0) = (\delta x_1(0), \delta x_2(0), \dots, \delta x_{2N}(0))$$

The evolution in time (in maps the time is discrete and is equal to the number  $n$  of the iterations) of a deviation vector is defined by:

- the variational equations (for Hamiltonian flows) and
- the equations of the tangent map (for mappings)

# Definition of the SALI

We follow the evolution in time of two different initial deviation vectors ( $v_1(0)$ ,  $v_2(0)$ ), and define SALI [S., J. Phys. A (2001) – S. & Manos, Lect. Notes Phys. (2016)] as:

$$SALI(t) = \min\{\|\hat{v}_1(t) + \hat{v}_2(t)\|, \|\hat{v}_1(t) - \hat{v}_2(t)\|\}$$

where

$$\hat{v}_1(t) = \frac{v_1(t)}{\|v_1(t)\|}$$

When the two vectors become collinear

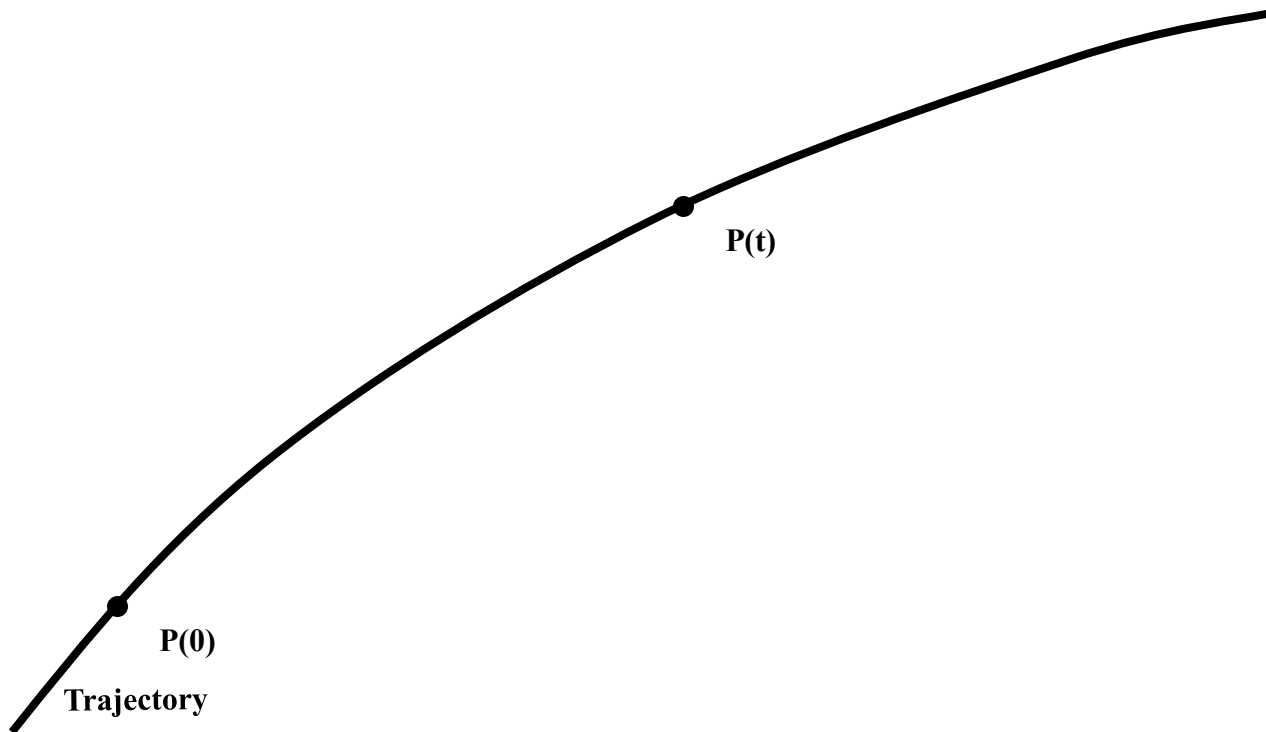
$$SALI(t) \rightarrow 0$$

# Behavior of SALI for **chaotic motion**

For chaotic orbits the two initially different deviation vectors tend to coincide with the direction defined by the maximum Lyapunov exponent.

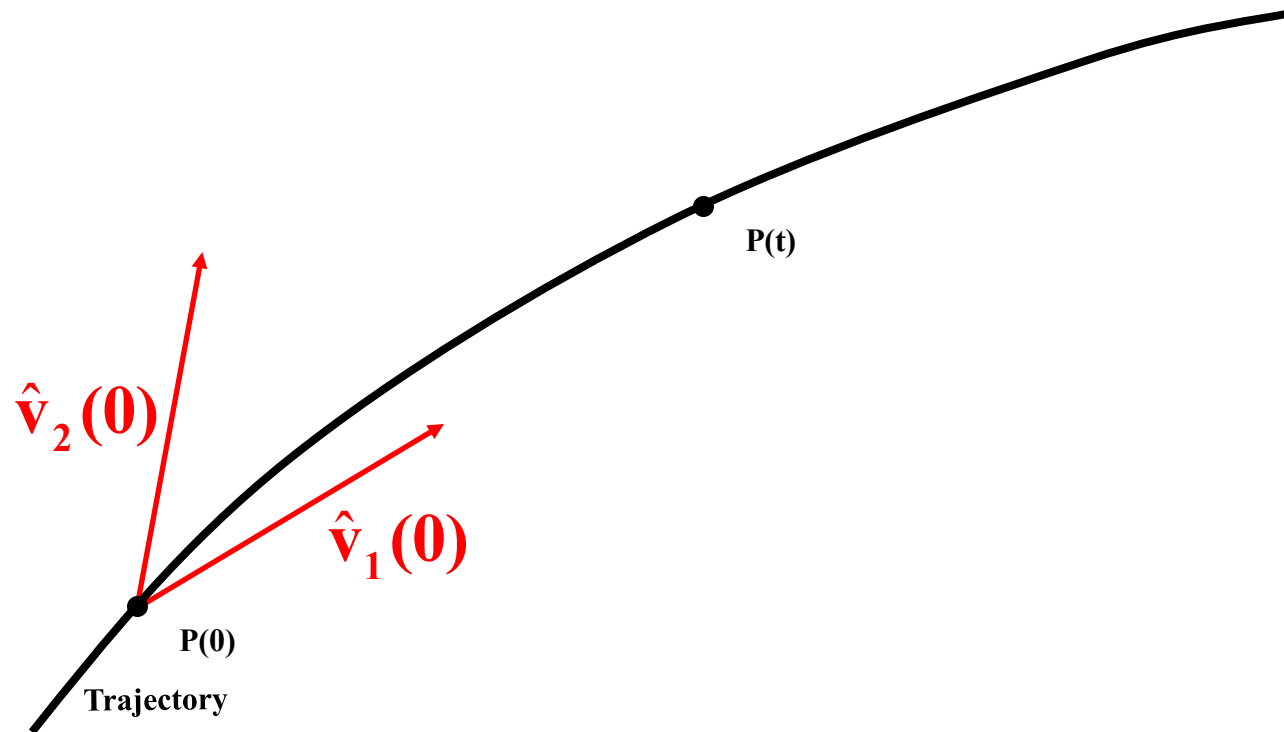
# Behavior of SALI for **chaotic motion**

For chaotic orbits the two initially different deviation vectors tend to coincide with the direction defined by the maximum Lyapunov exponent.



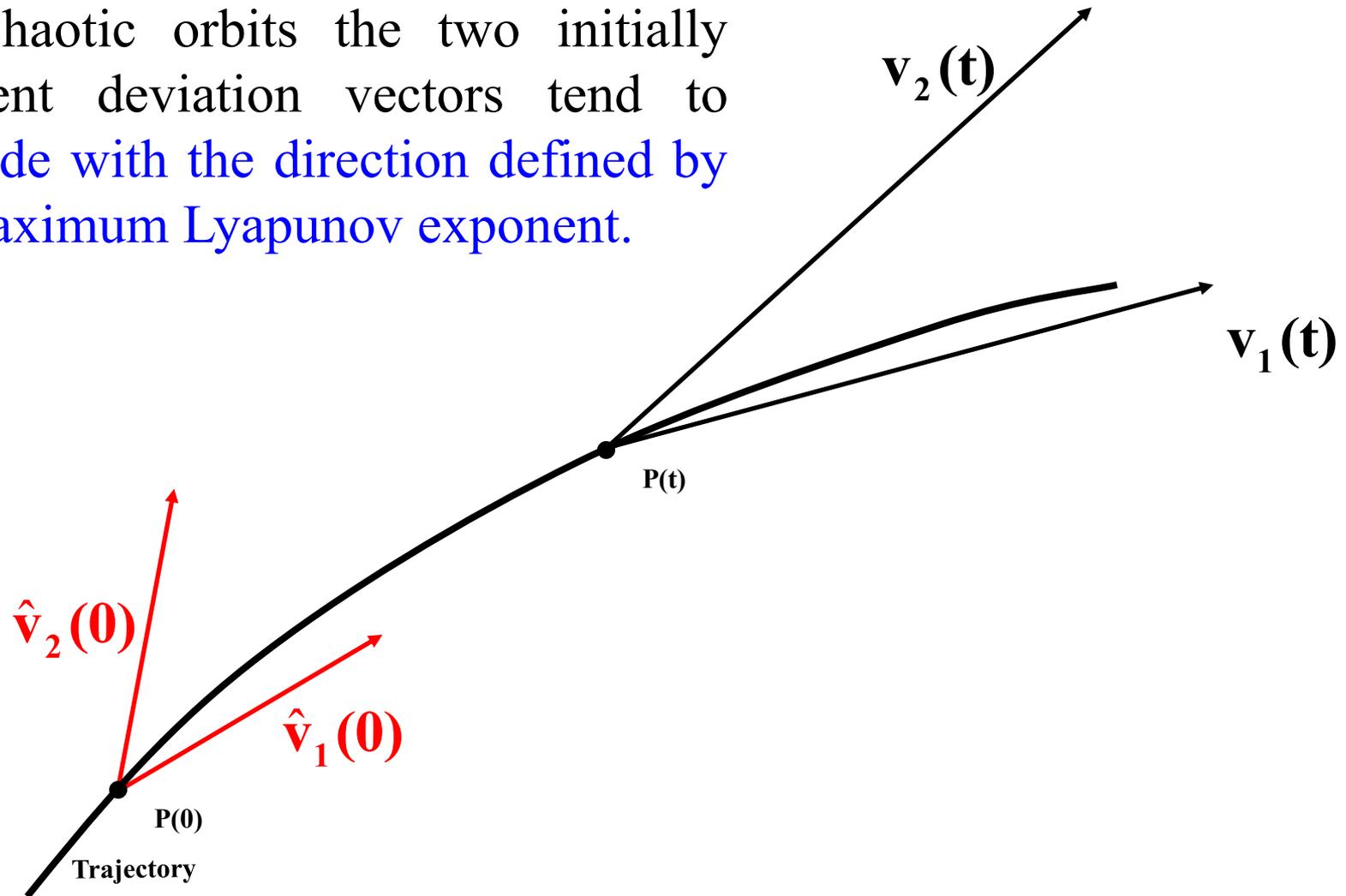
# Behavior of SALI for **chaotic motion**

For chaotic orbits the two initially different deviation vectors tend to coincide with the direction defined by the maximum Lyapunov exponent.



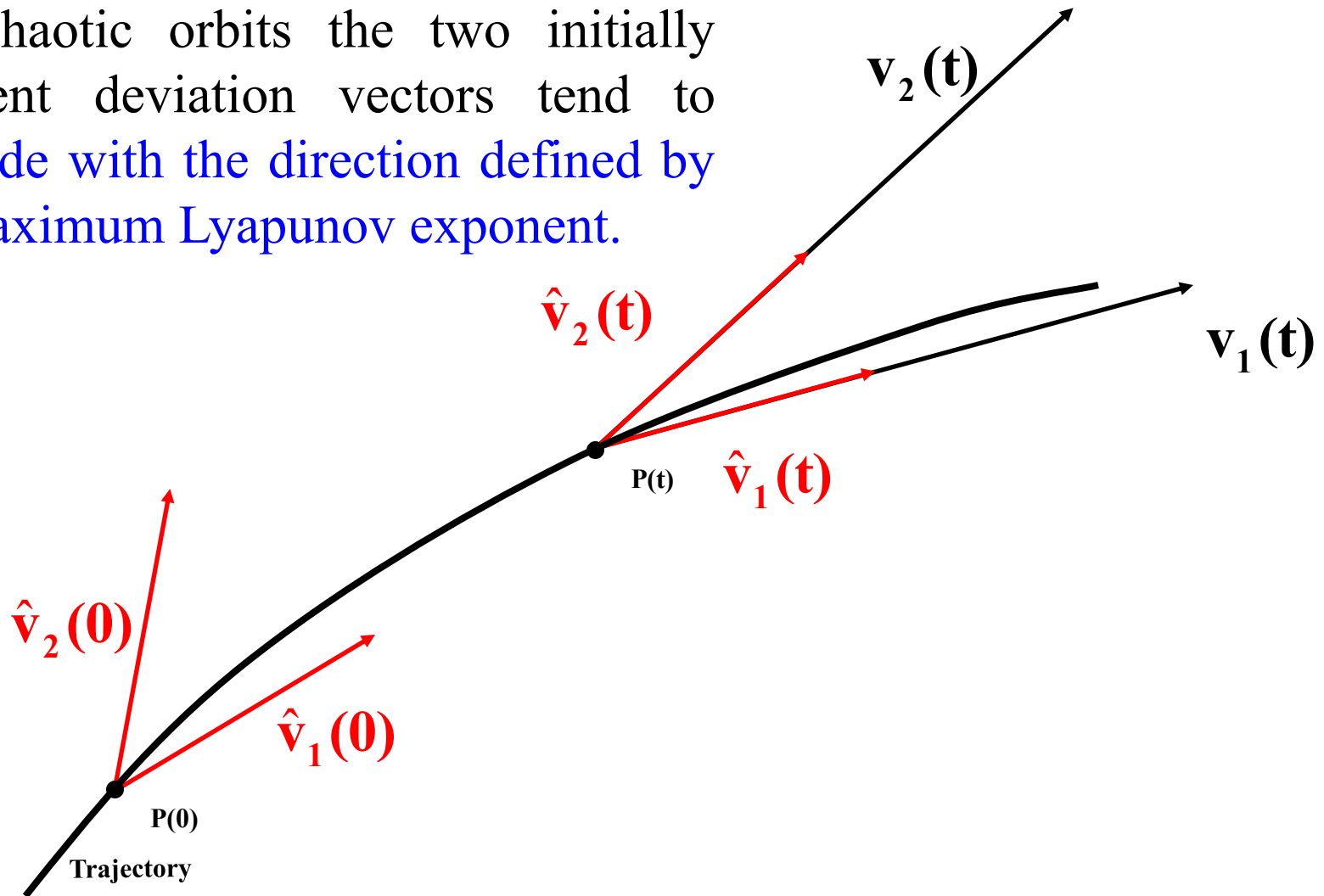
# Behavior of SALI for **chaotic motion**

For chaotic orbits the two initially different deviation vectors tend to coincide with the direction defined by the maximum Lyapunov exponent.



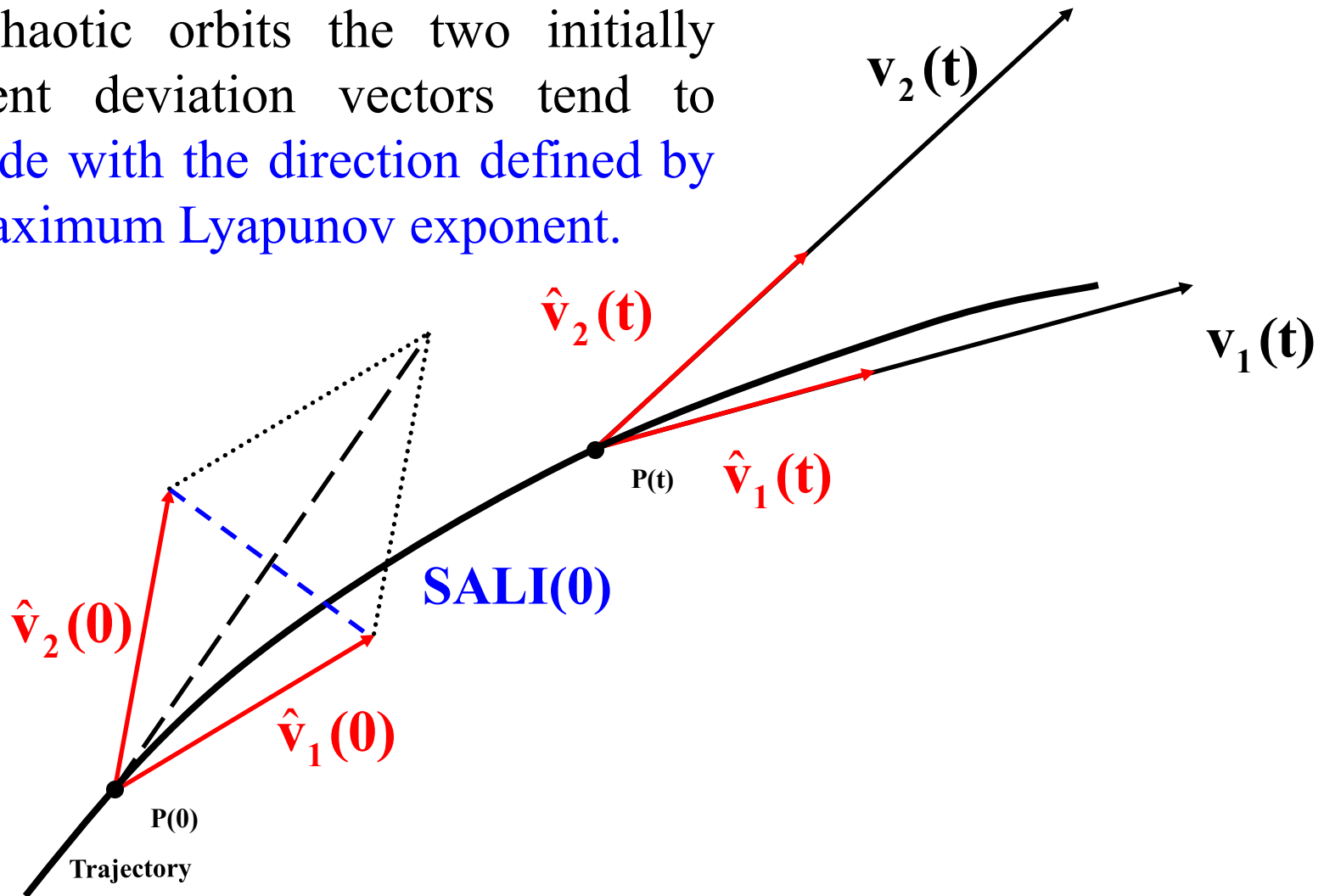
# Behavior of SALI for **chaotic motion**

For chaotic orbits the two initially different deviation vectors tend to coincide with the direction defined by the maximum Lyapunov exponent.



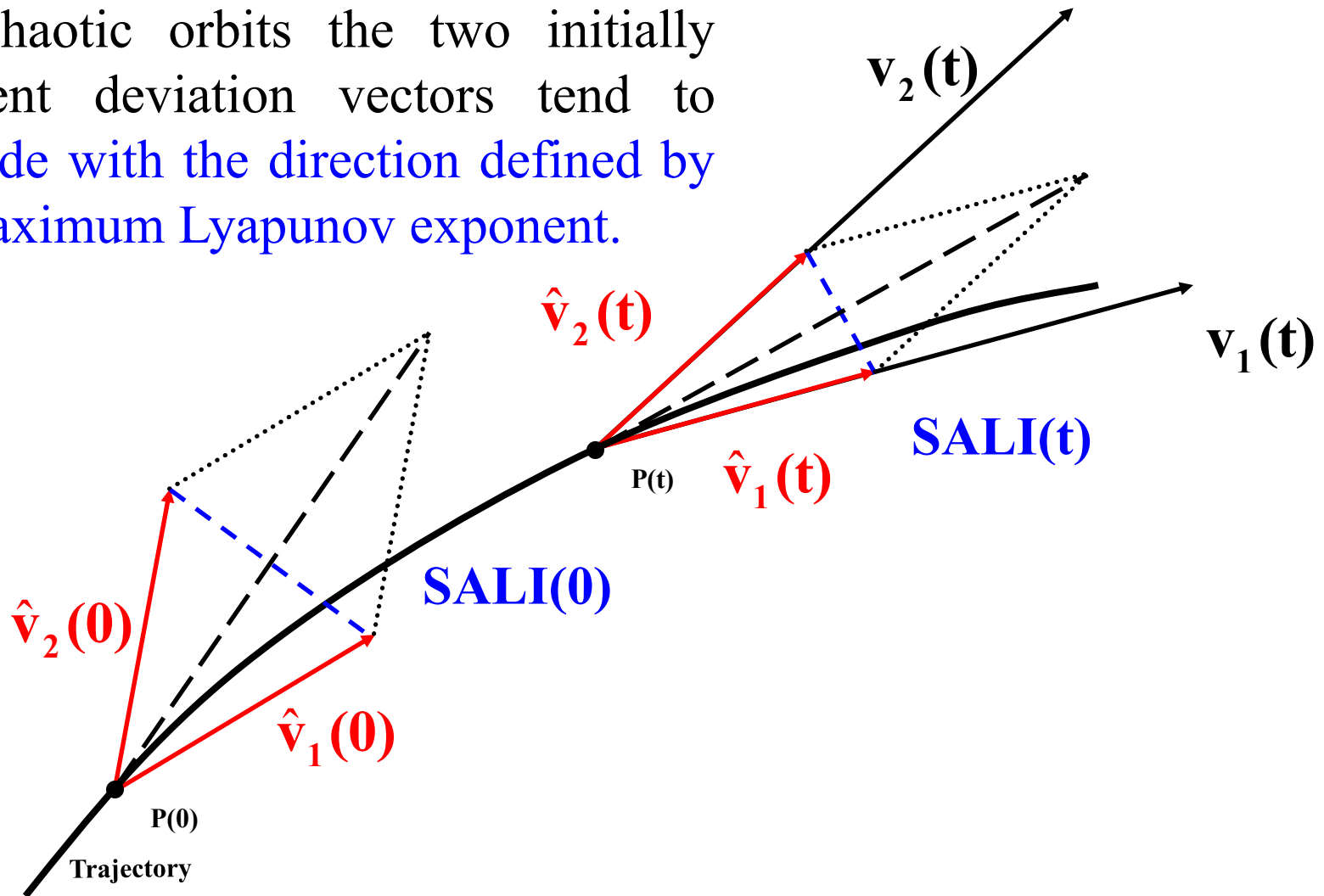
# Behavior of SALI for chaotic motion

For chaotic orbits the two initially different deviation vectors tend to coincide with the direction defined by the maximum Lyapunov exponent.



# Behavior of SALI for chaotic motion

For chaotic orbits the two initially different deviation vectors tend to coincide with the direction defined by the maximum Lyapunov exponent.

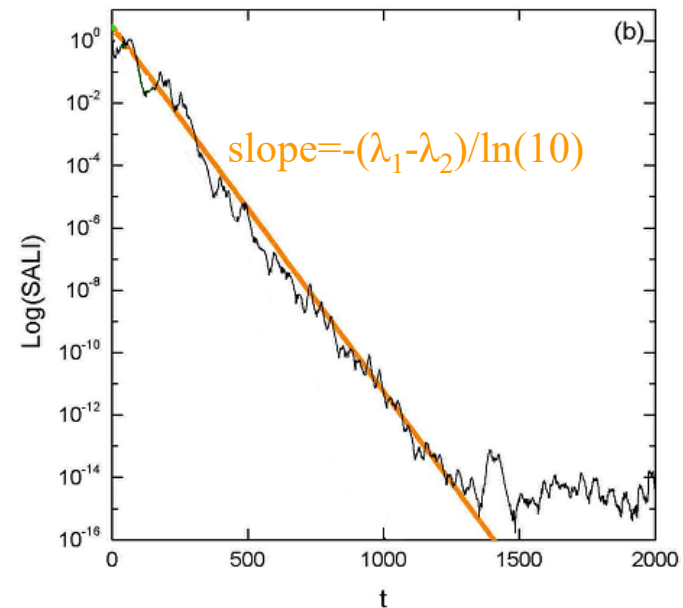
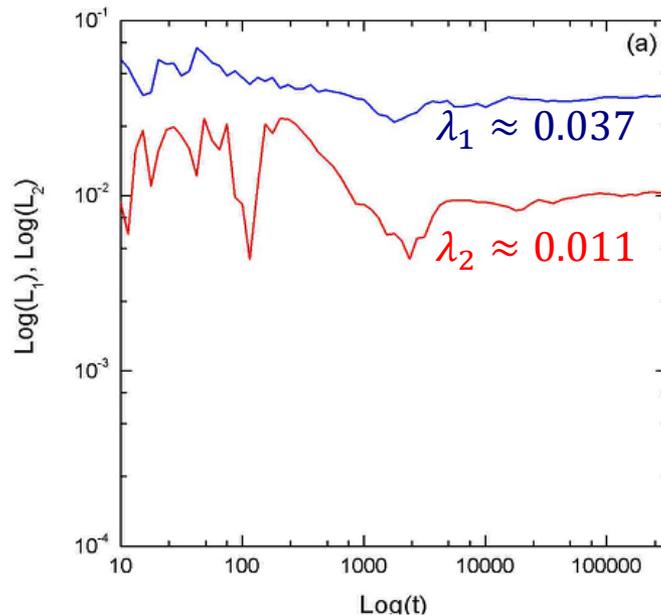


# Behavior of the SALI for chaotic motion

We test the validity of the approximation  $SALI \propto e^{-(\lambda_1 - \lambda_2)t}$  [S. et al., J. Phys. A (2004)] for a chaotic orbit of the 3D Hamiltonian

$$H = \sum_{i=1}^3 \frac{\omega_i}{2} (q_i^2 + p_i^2) + q_1^2 q_2 + q_1^2 q_3$$

with  $\omega_1=1$ ,  $\omega_2=1.4142$ ,  $\omega_3=1.7321$ ,  $H=0.09$

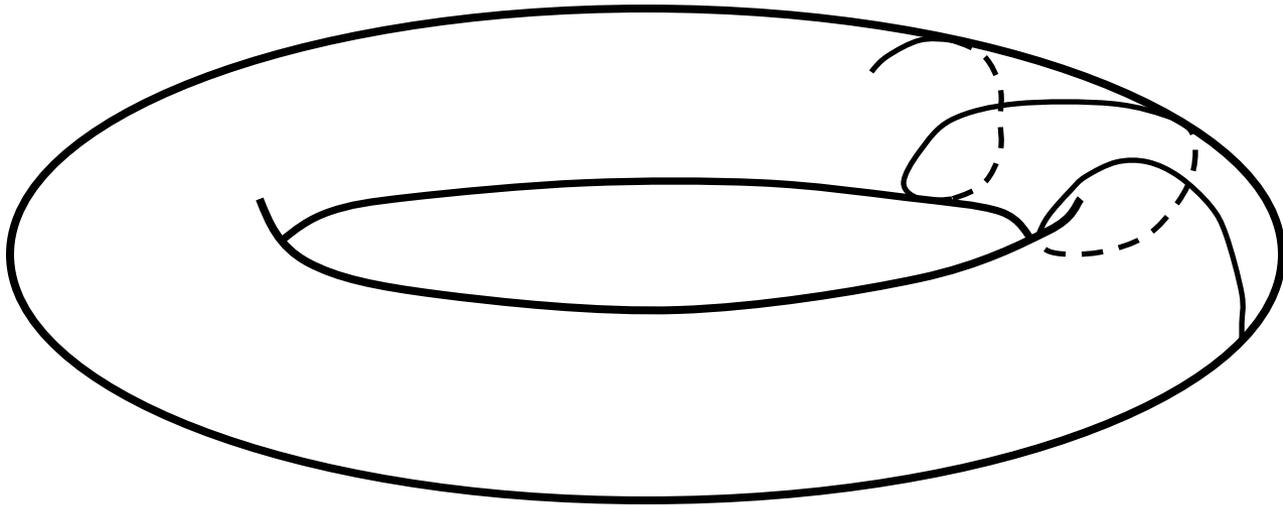


# Behavior of SALI for regular motion

Regular motion occurs on a torus and two different initial deviation vectors become tangent to the torus, generally having different directions.

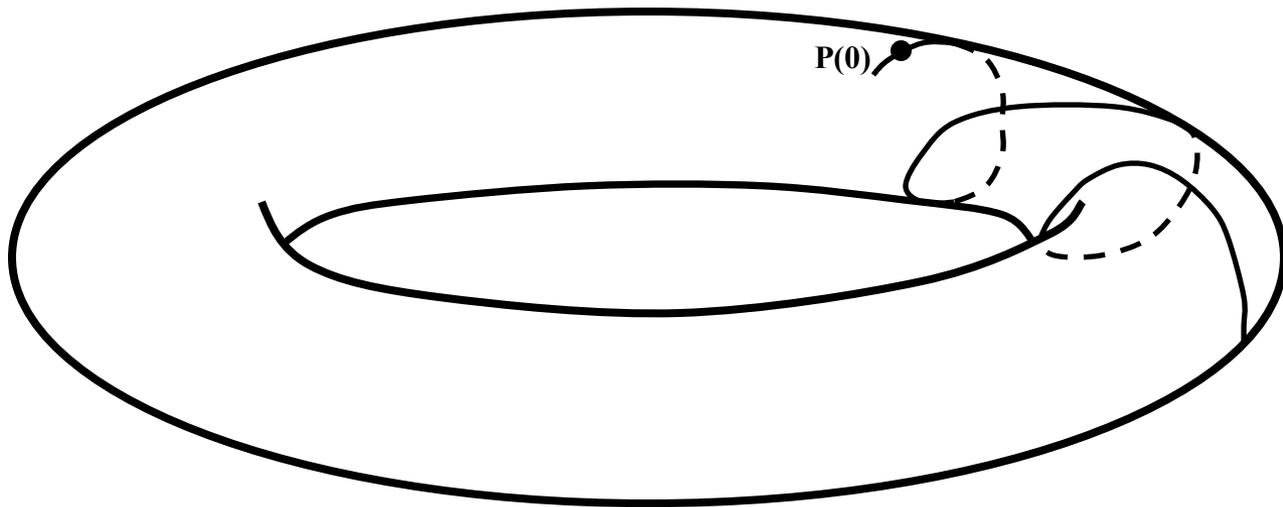
# Behavior of SALI for **regular motion**

Regular motion occurs on a torus and two different initial deviation vectors **become tangent to the torus, generally having different directions.**



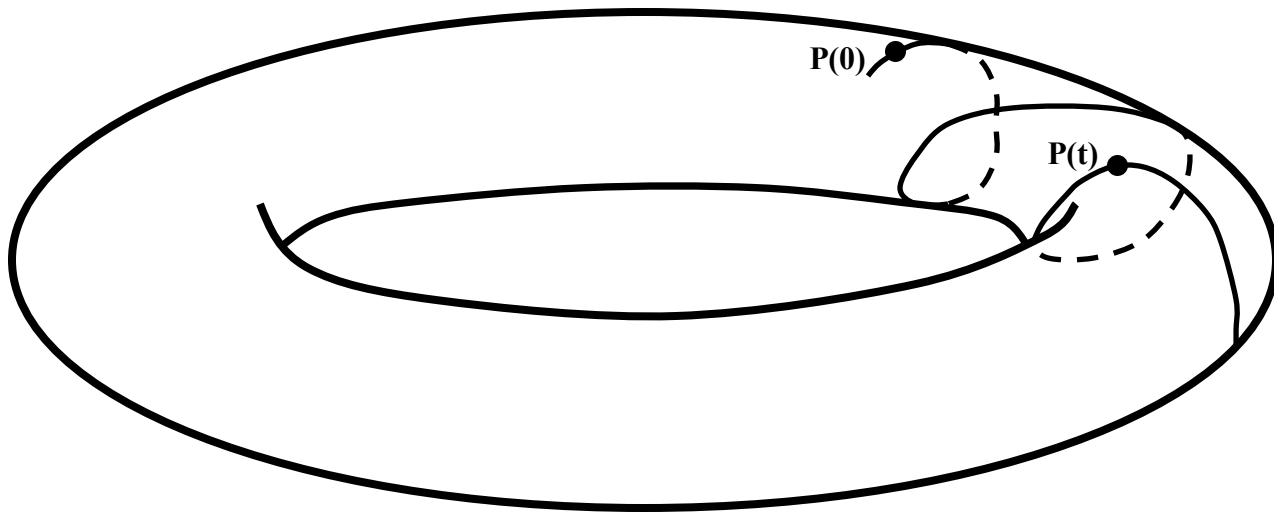
# Behavior of SALI for **regular motion**

Regular motion occurs on a torus and two different initial deviation vectors **become tangent to the torus, generally having different directions.**



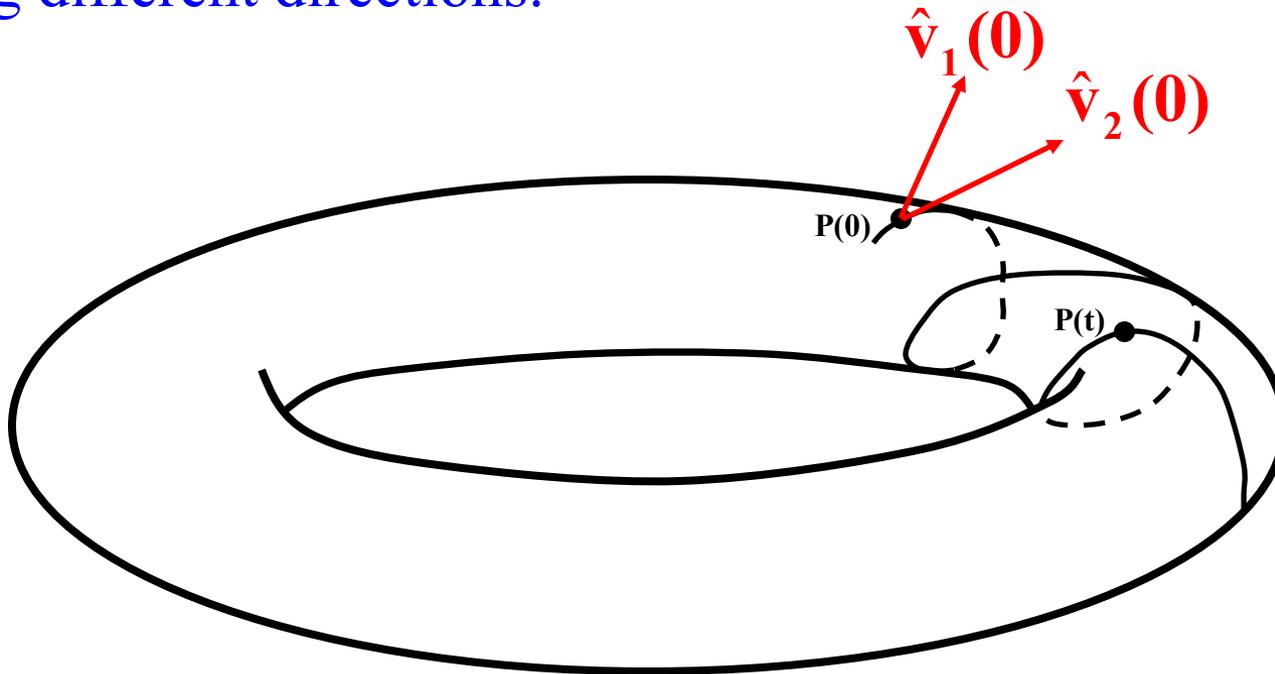
# Behavior of SALI for **regular motion**

Regular motion occurs on a torus and two different initial deviation vectors **become tangent to the torus, generally having different directions.**



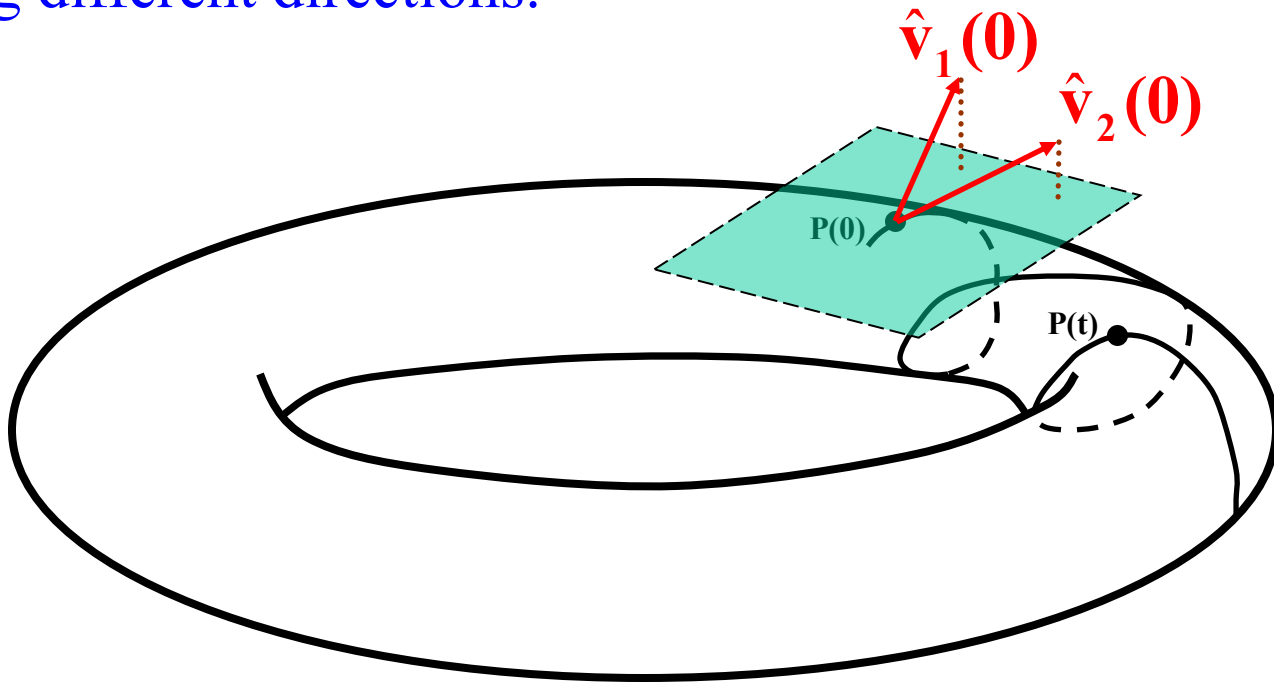
# Behavior of SALI for **regular motion**

Regular motion occurs on a torus and two different initial deviation vectors **become tangent to the torus**, generally having different directions.



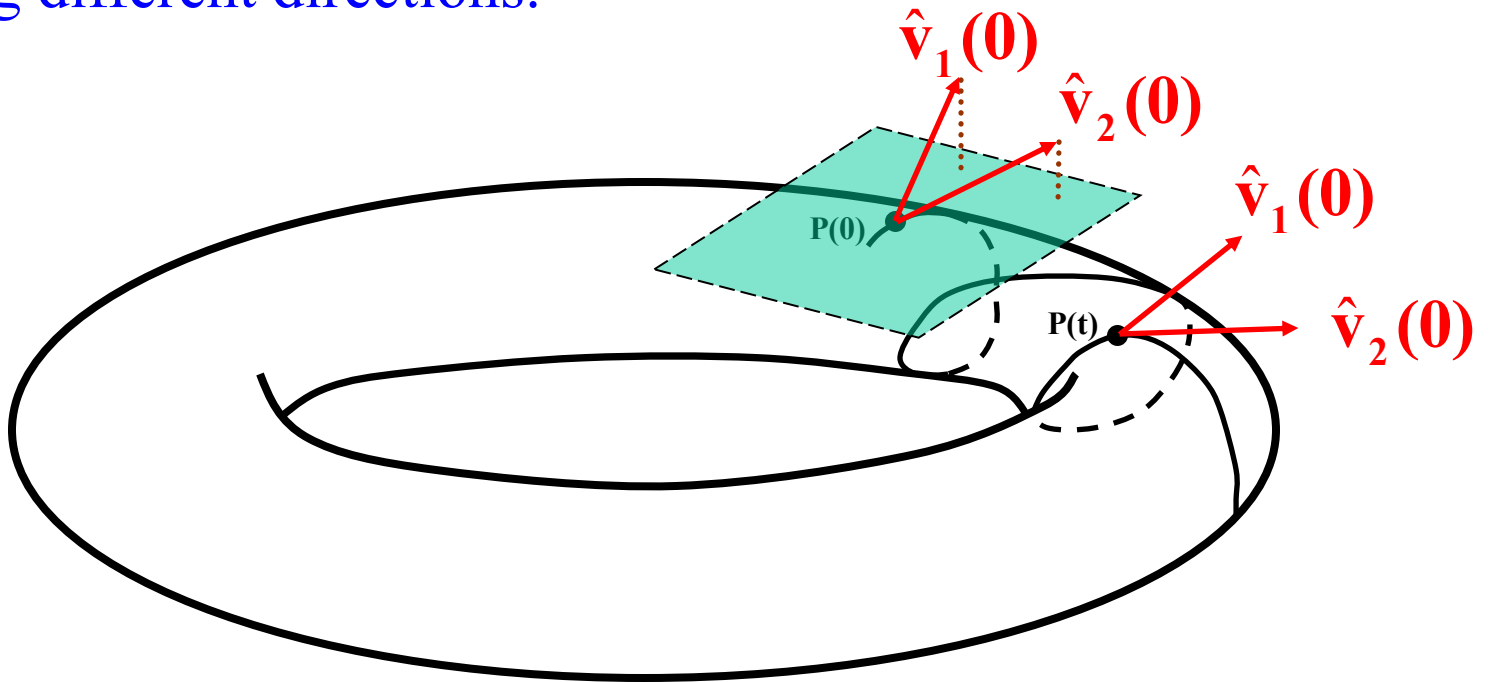
# Behavior of SALI for regular motion

Regular motion occurs on a torus and two different initial deviation vectors become tangent to the torus, generally having different directions.



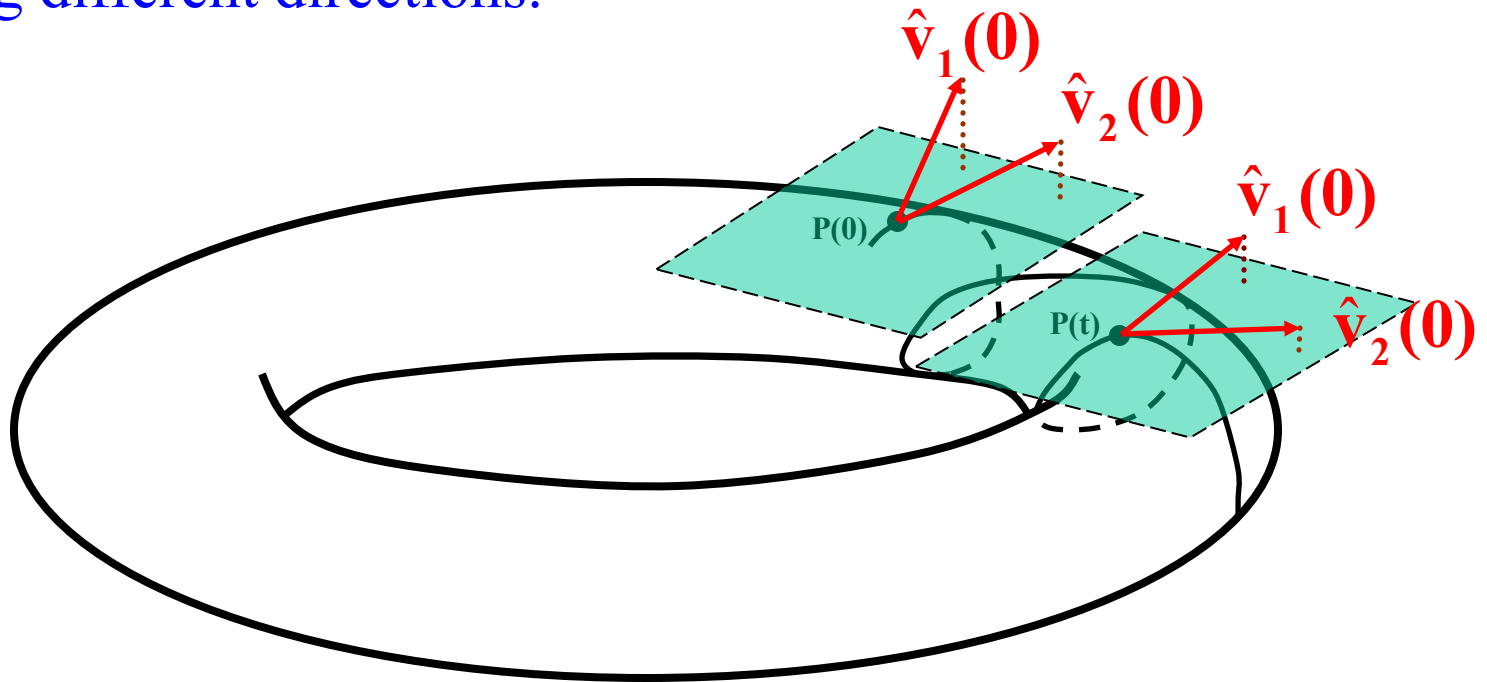
# Behavior of SALI for regular motion

Regular motion occurs on a torus and two different initial deviation vectors become tangent to the torus, generally having different directions.



# Behavior of SALI for regular motion

Regular motion occurs on a torus and two different initial deviation vectors become tangent to the torus, generally having different directions.



# SALI – Hénon-Heiles system

As an example, we consider the 2D Hénon-Heiles system:

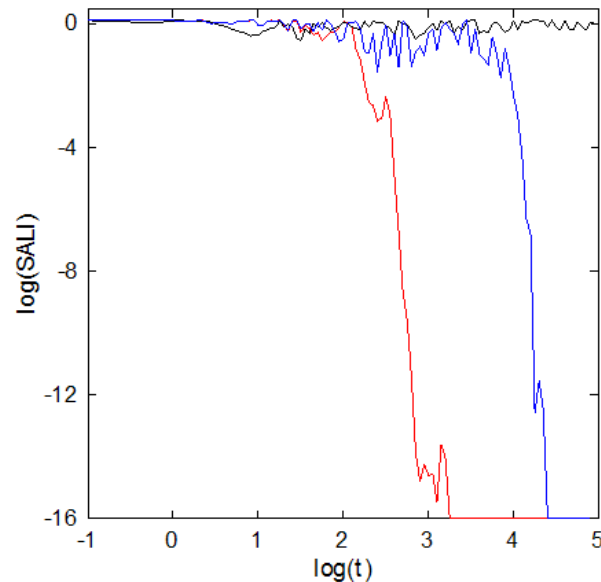
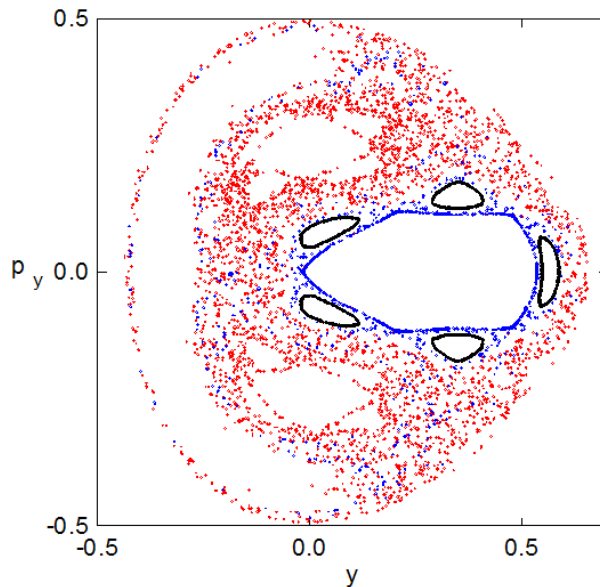
$$H = \frac{1}{2}(p_x^2 + p_y^2) + \frac{1}{2}(x^2 + y^2) + x^2y - \frac{1}{3}y^3$$

For  $E=1/8$  we consider the orbits with initial conditions:

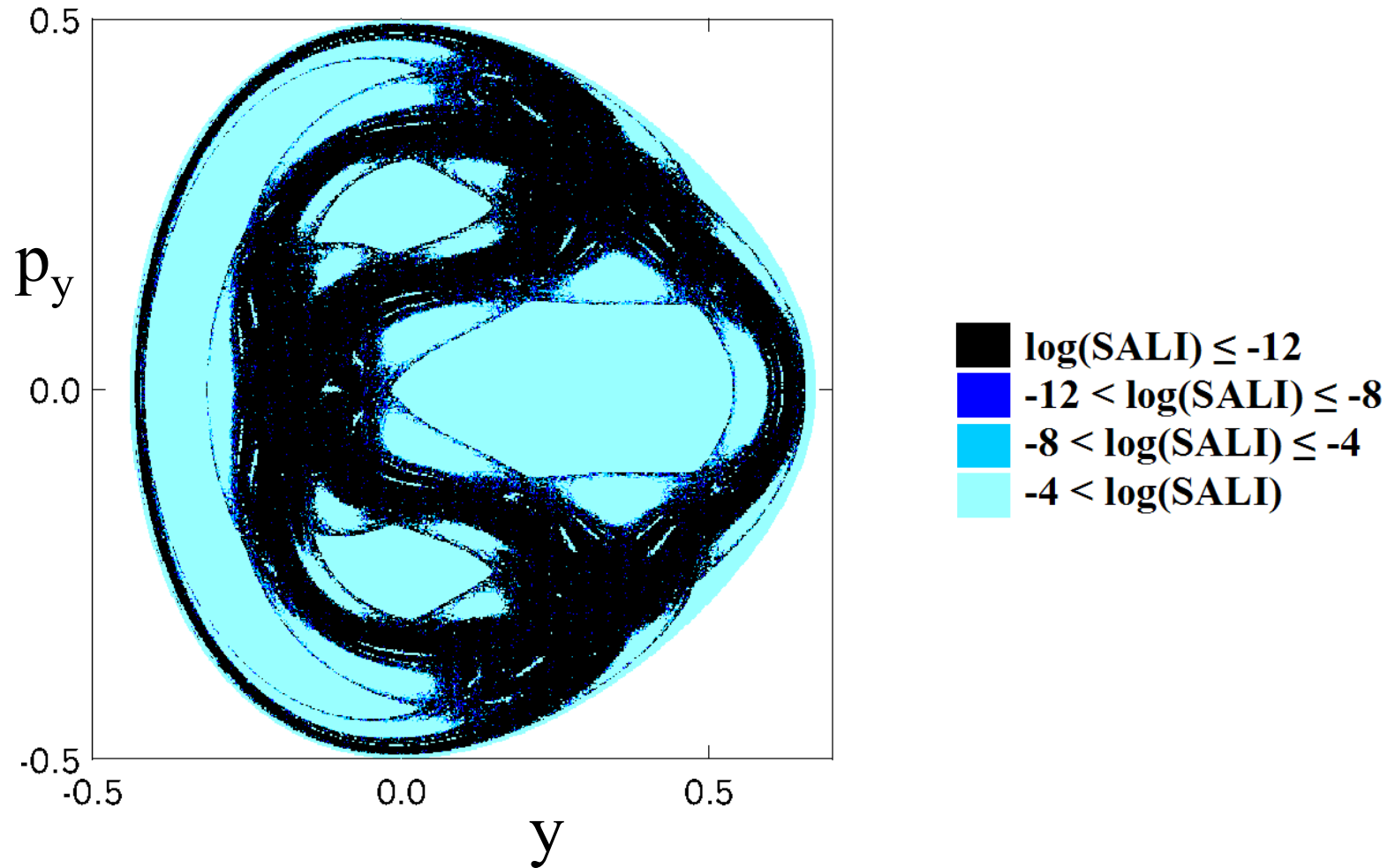
Regular orbit,  $x=0, y=0.55, p_x=0.2417, p_y=0$

Chaotic orbit,  $x=0, y=-0.016, p_x=0.49974, p_y=0$

Chaotic orbit,  $x=0, y=-0.01344, p_x=0.49982, p_y=0$



# SALI – Hénon-Heiles system



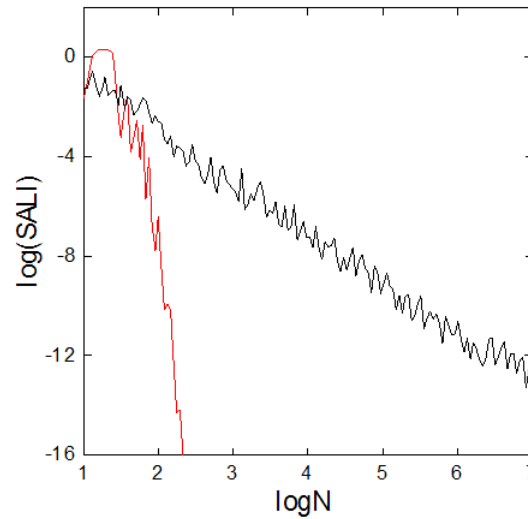
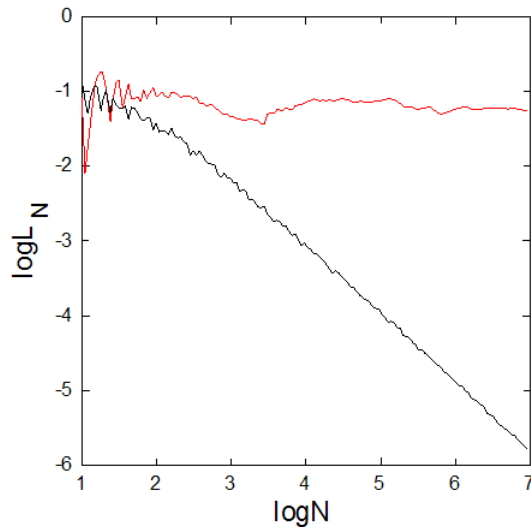
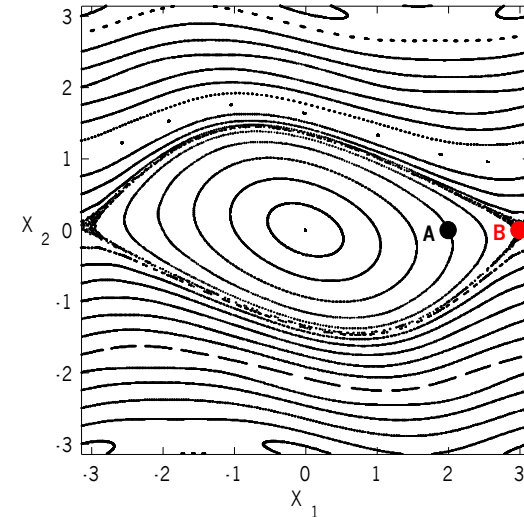
# Applications – 2D map

$$\begin{aligned}x_1' &= x_1 + x_2 \\x_2' &= x_2 - \nu \sin(x_1 + x_2)\end{aligned}\quad (\text{mod } 2\pi)$$

For  $\nu=0.5$  we consider the orbits:

regular orbit A with initial conditions  $x_1=2, x_2=0$ .

chaotic orbit B with initial conditions  $x_1=3, x_2=0$ .



# Behavior of the SALI

2D maps

SALI  $\rightarrow 0$  both for regular and chaotic orbits

following, however, completely different time rates which allows us to distinguish between the two cases.

Hamiltonian flows and multidimensional maps

SALI  $\rightarrow 0$  for chaotic orbits

SALI  $\rightarrow \text{constant} \neq 0$  for regular orbits

# Using LDs to quantify chaos

We consider orbits on a finite grid of an  $n(\geq 1)$ -dimensional subspace of the  $N(\geq n)$ -dimensional phase space of a dynamical system and their LDs.

Any non-boundary point  $x$  in this subspace has  $2n$  nearest neighbors

$$y_i^\pm = x \pm \sigma^{(i)} e^{(i)}, \quad i = 1, 2, \dots, n,$$

where  $e^{(i)}$  is the  $i$ th usual basis vector in  $\mathbb{R}^n$  and  $\sigma^{(i)}$  is the distance between successive grid points in this direction.

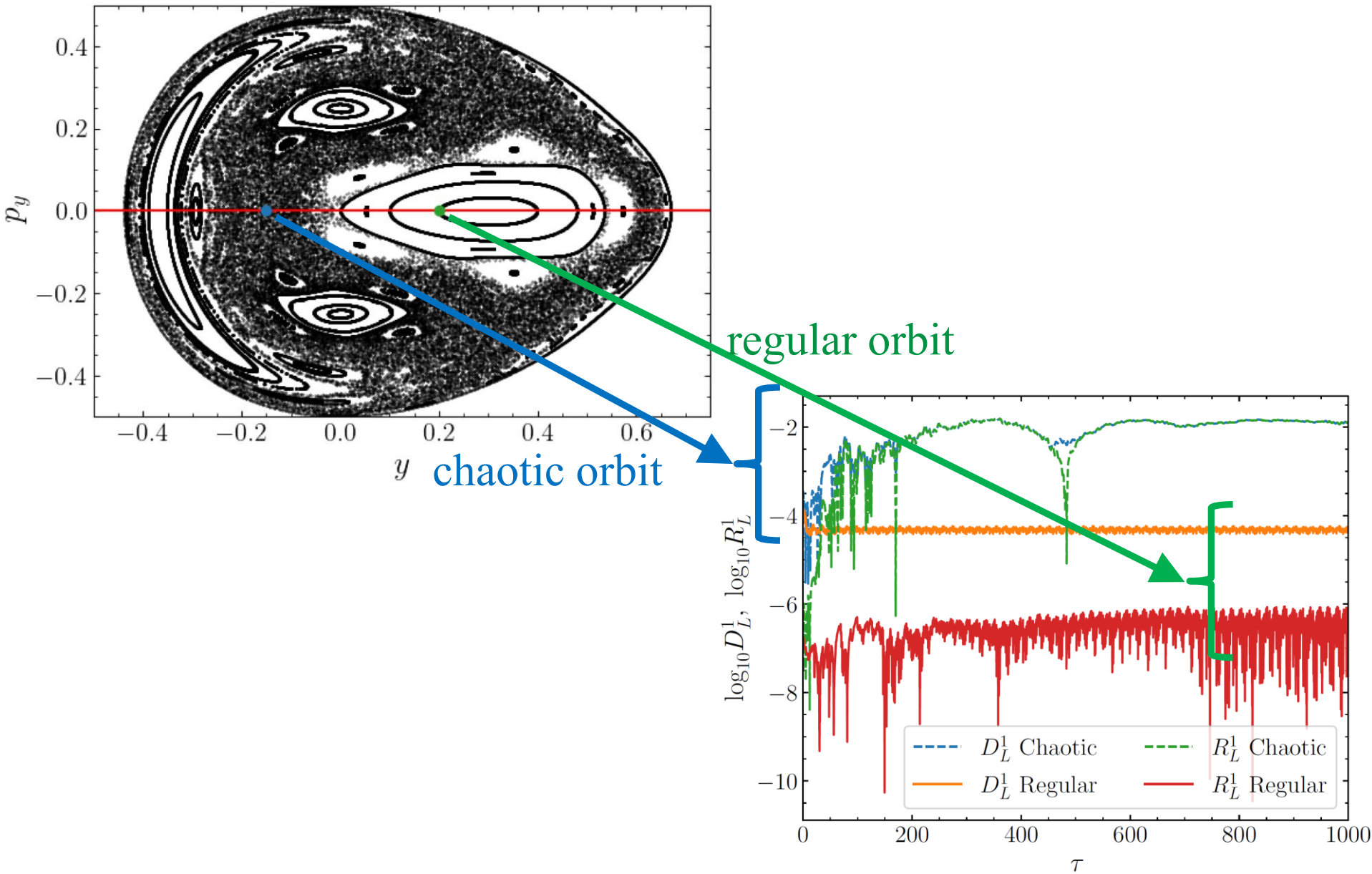
The **difference**  $D_L^n$  of neighboring orbits' LDs:

$$D_L^n(x) = \frac{1}{2n} \sum_{i=1}^n \frac{|LD^f(x) - LD^f(y_i^+)| + |LD^f(x) - LD^f(y_i^-)|}{LD^f(x)}.$$

The **ratio**  $R_L^n$  of neighboring orbits' LDs:

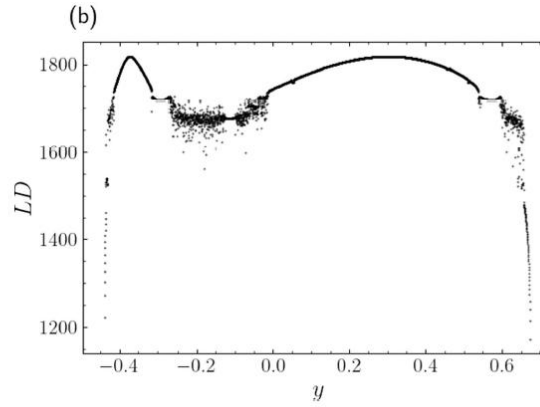
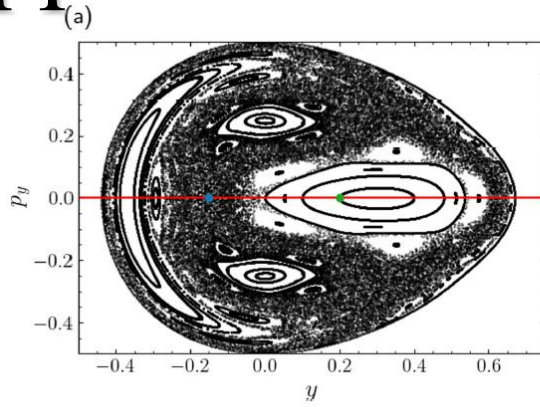
$$R_L^n(x) = \left| 1 - \frac{1}{2n} \sum_{i=1}^n \frac{LD^f(y_i^+) + LD^f(y_i^-)}{LD^f(x)} \right|.$$

# Application: Hénon-Heiles system



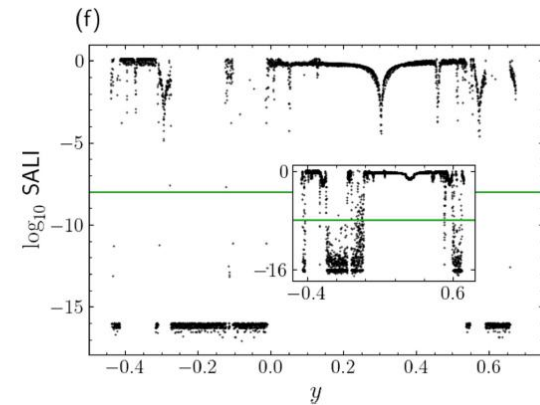
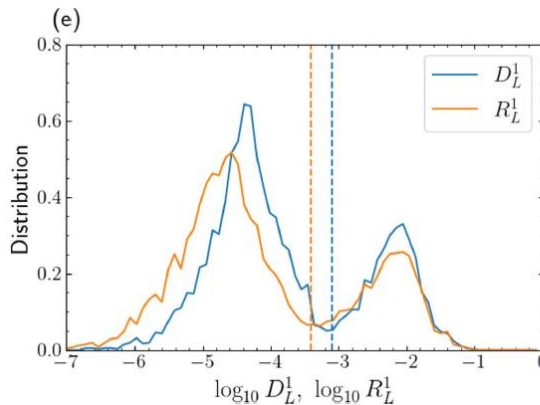
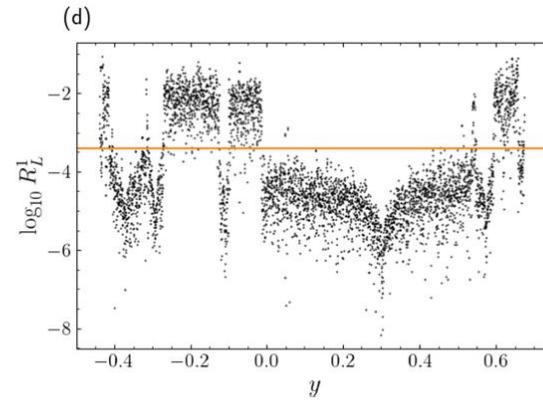
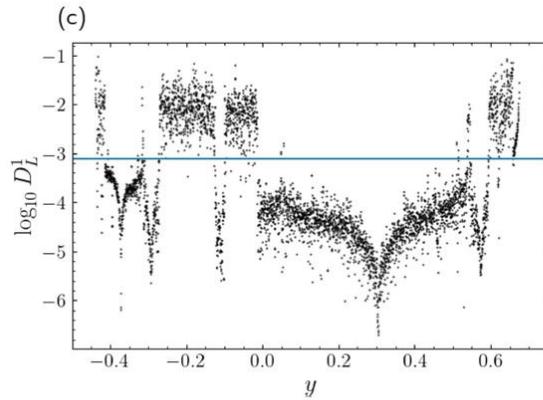
# Application: Hénon-Heiles system

H=1/8



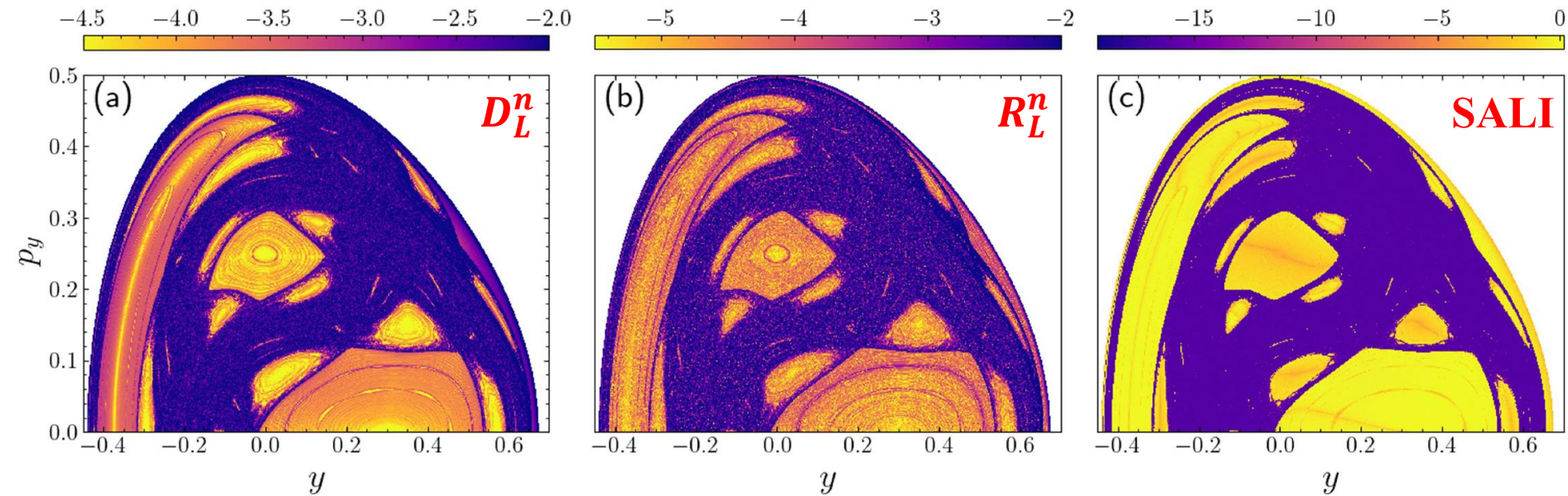
Variation of LDs with regard to initial conditions.  
regular regions: smooth  
chaotic regions: erratic  
[also see Montes et al., Commun. Nonlin. Sci. Num. Simul. (2021)]

LDs for  $\tau=10^3$

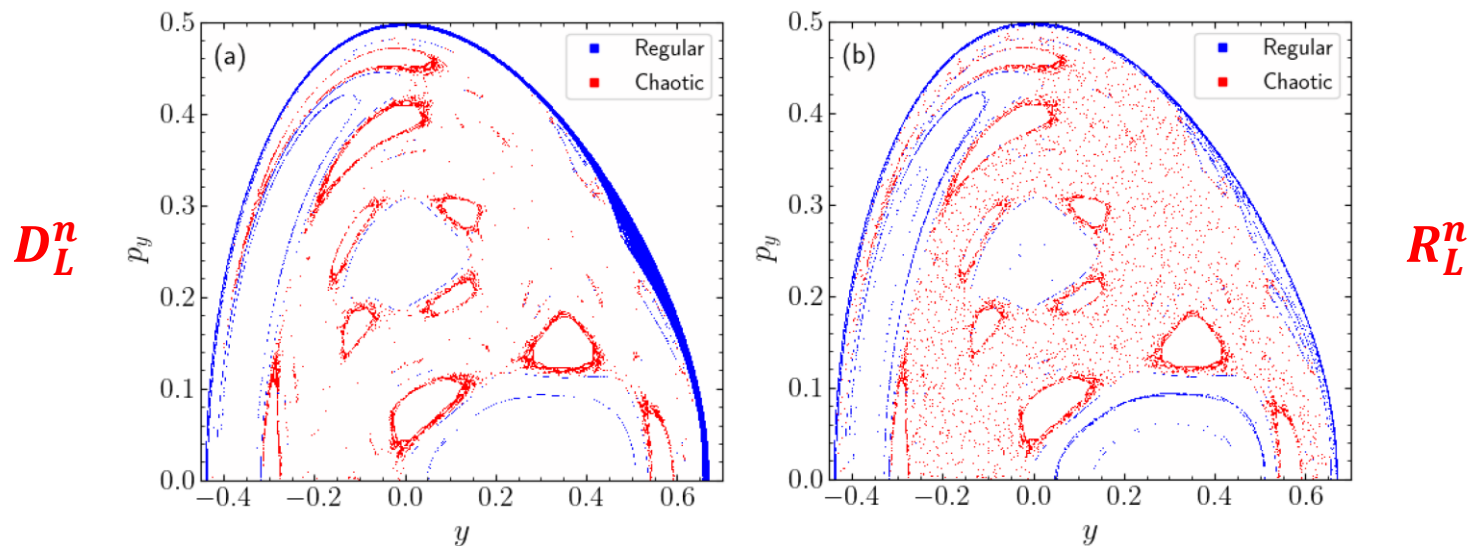


SALI for  $\tau=10^6$   
(inset  $\tau=10^3$ )

# Application: Hénon-Heiles system



Misclassified orbits (< 10%)



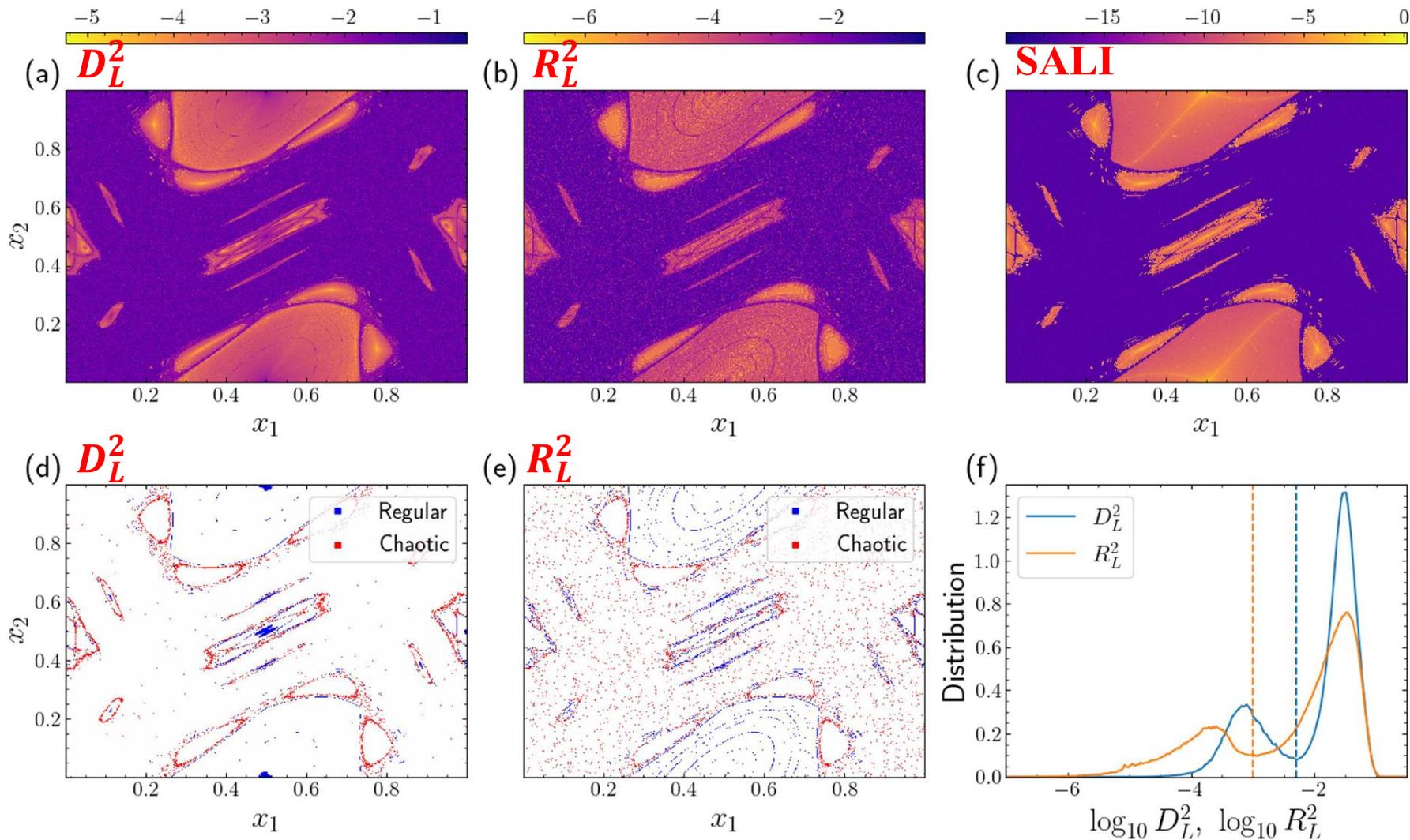
# Application: 2D Standard map

$$\begin{aligned}x'_1 &= x_1 + x'_2 \\x'_2 &= x_2 + \frac{K}{2\pi} \sin(2\pi x_1) \pmod{1}\end{aligned}$$

We set  $K = 1.5$

Thresholds:  $\log_{10} D_L^2 = -2.3$ ,  $\log_{10} R_L^2 = -3$  ( $T = 10^3$ )

$\log_{10} \text{SALI} = -12$  ( $T = 10^5$ )

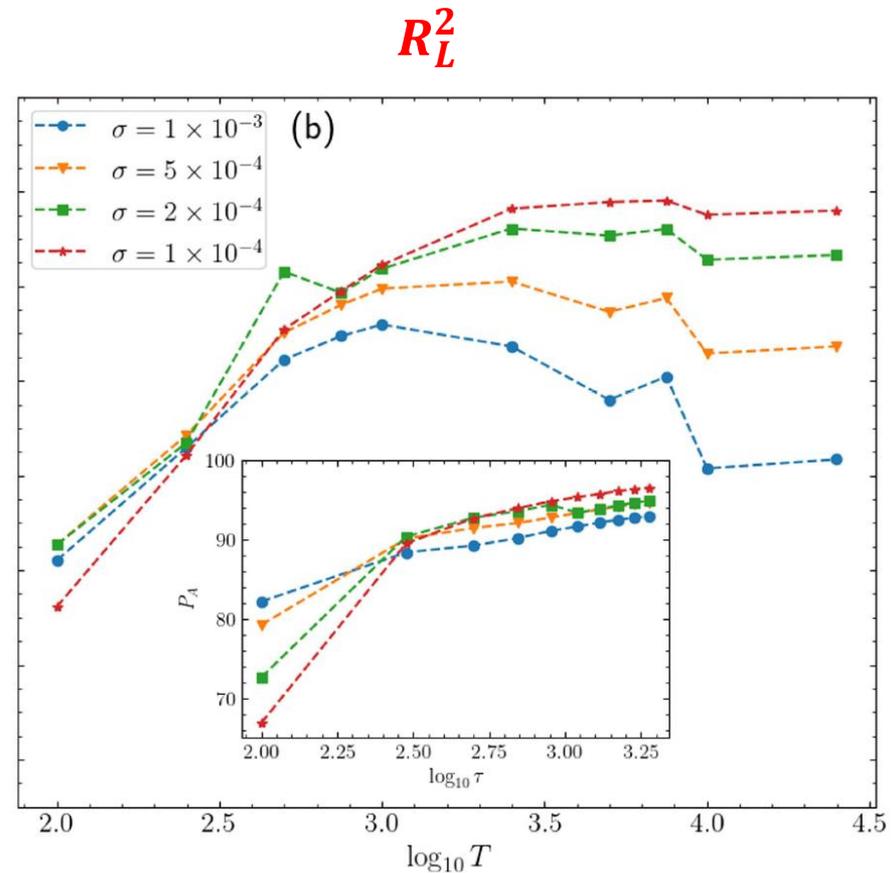
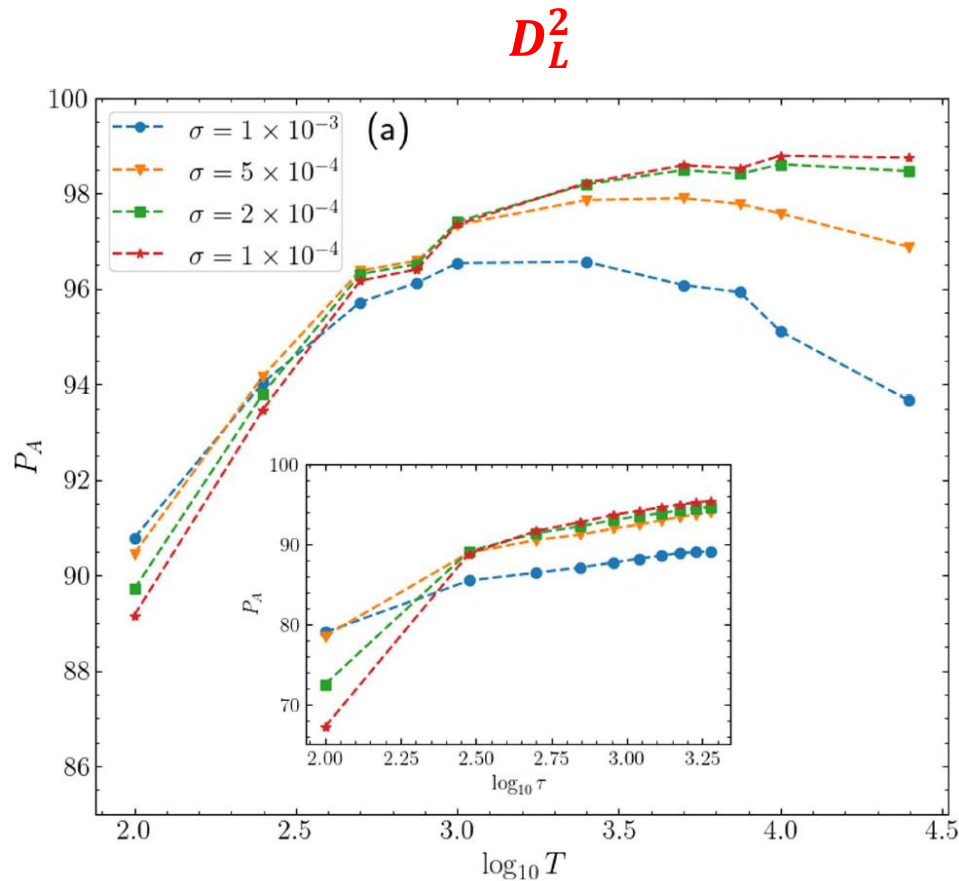


# Effect of grid spacing ( $\sigma$ ) and final integration time ( $T, \tau$ )

$P_A$  : percentage of correctly characterized orbits

Main plots: 2D Standard map

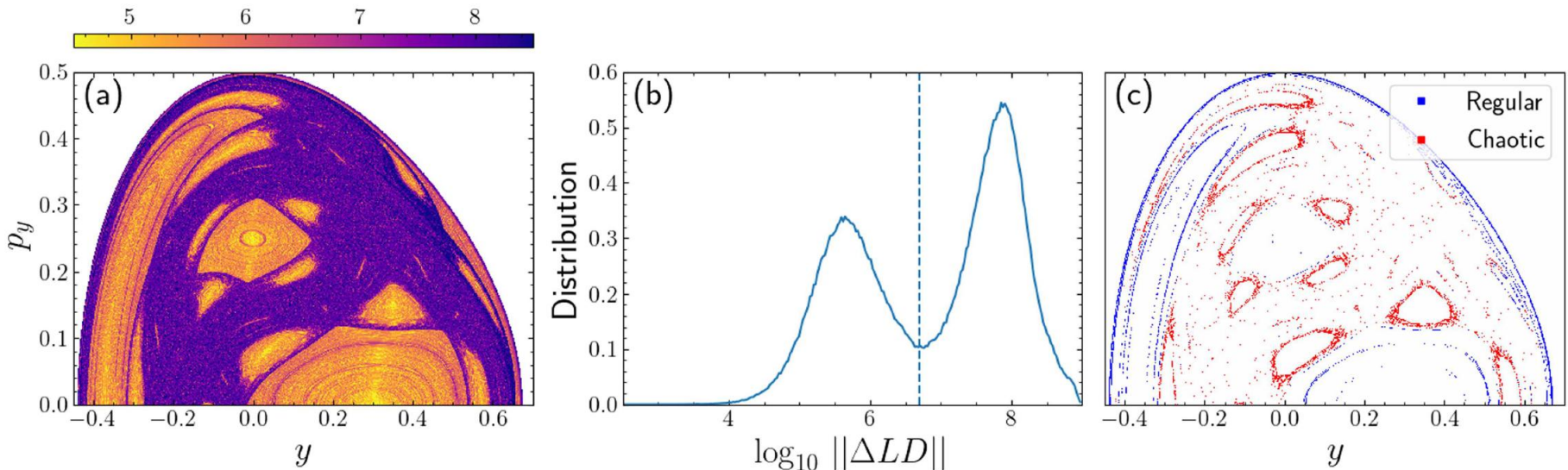
Insets: Hénon-Heiles system



# Application: Hénon-Heiles system

A quantity related to **the second spatial derivative of the LDs** was introduced in Daquin et al., Physica D (2022) and was used in Hillebrand et al., Chaos (2022):

$$\|\Delta LD\|(x) = \left| \frac{LD^f(y_i^+) - 2LD^f(x) + LD^f(y_i^-)}{\sigma^2} \right|.$$

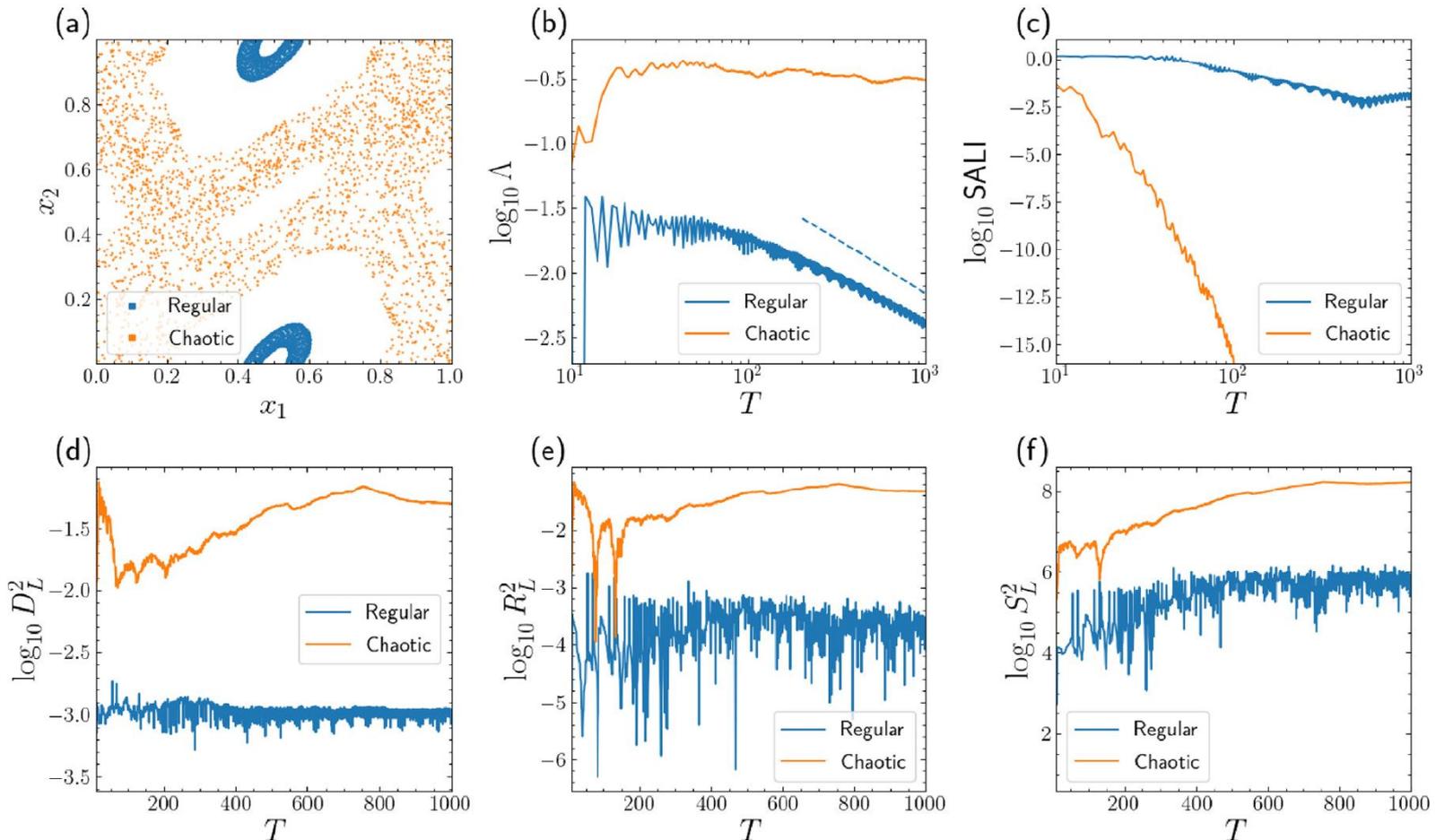


In Zimmer et al., Physica D (2023) it was modified to:

$$S_L^n(x) = \frac{1}{n} \sum_{i=1}^n \left| \frac{LD^f(y_i^+) - 2LD^f(x) + LD^f(y_i^-)}{(\sigma^{(i)})^2} \right|.$$

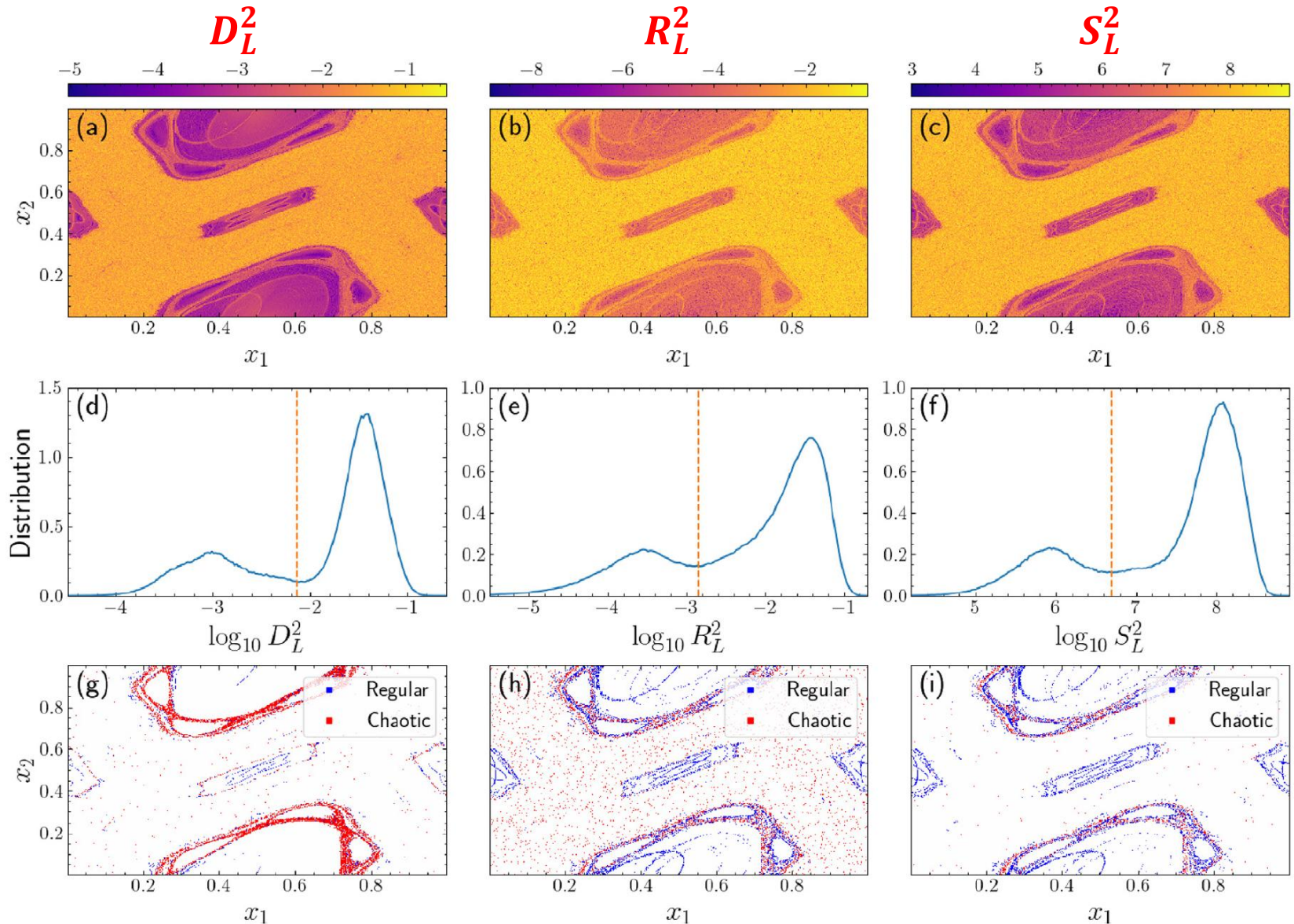
# Application: 4D Standard map

$$\begin{aligned}
 x'_1 &= x_1 + x'_2 \\
 x'_2 &= x_2 + \frac{K}{2\pi} \sin(2\pi x_1) - \frac{B}{2\pi} \sin[2\pi(x_3 - x_1)] \\
 x'_3 &= x_3 + x'_4 \\
 x'_4 &= x_4 + \frac{K}{2\pi} \sin(2\pi x_3) - \frac{B}{2\pi} \sin[2\pi(x_1 - x_3)]
 \end{aligned}
 \quad (\text{mod } 1)$$



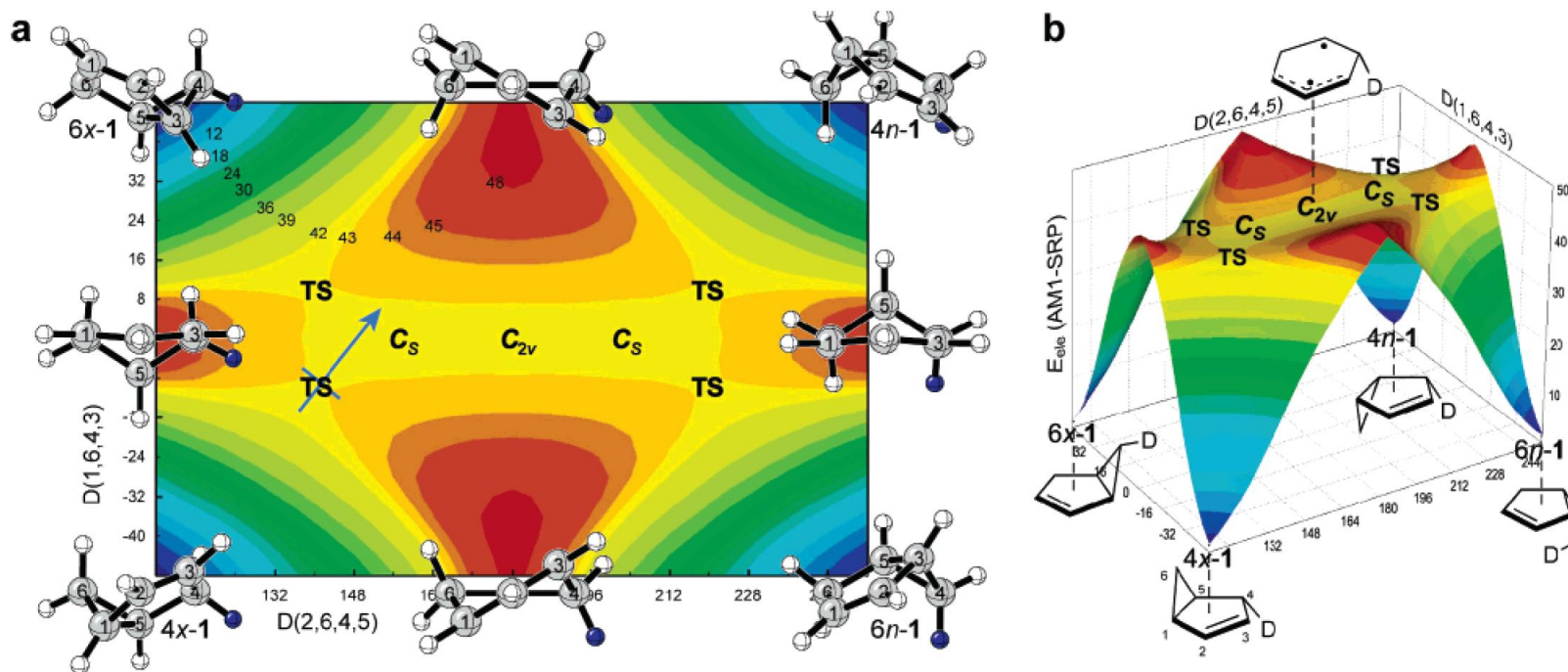
# Application: 4D Standard map

2D subspace  $(x_1, x_2)$  with  $x_3 = 0.54$ ,  $x_4 = 0.01$  for  $K = 1.5$ ,  $B = 0.05$  and  $T = 10^3$



# The caldera potential energy surface

Caldera type potentials, having a potential energy plateau, describe organic chemistry reactions.



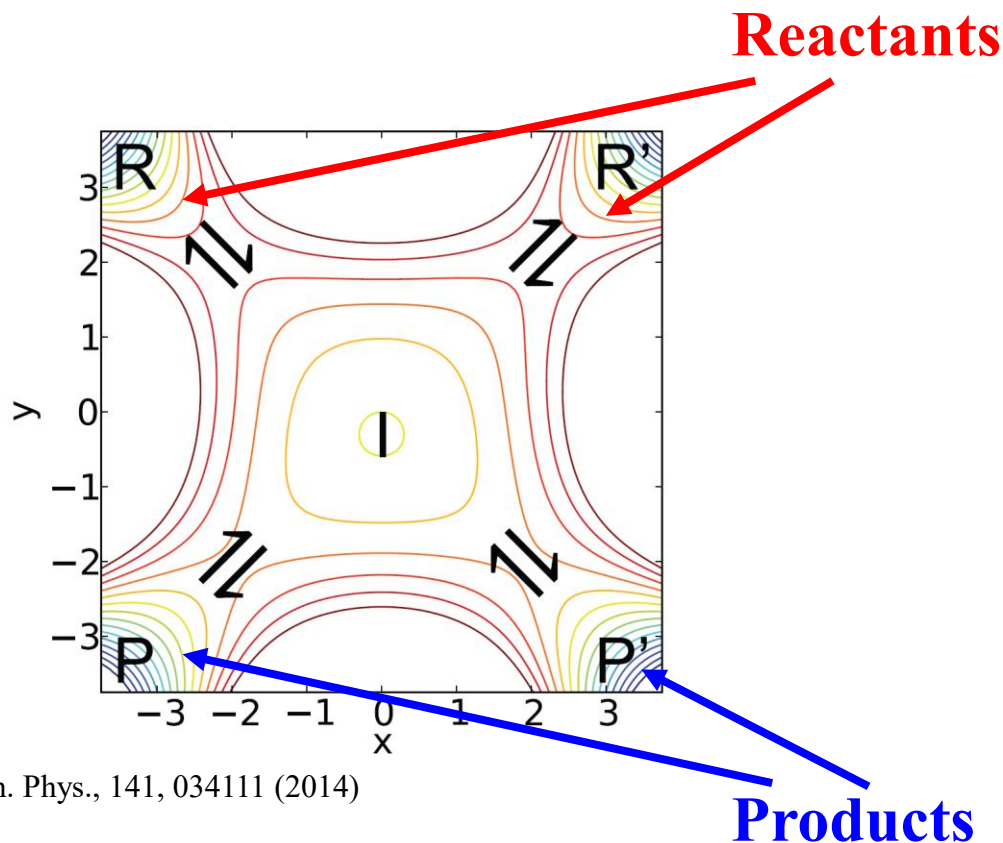
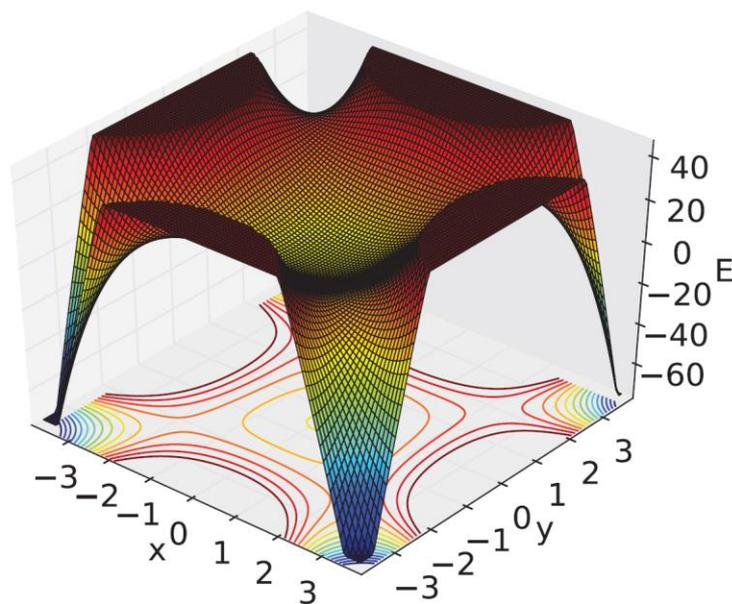
From Doubleday, Suhrada, Houk., *J. Am. Chem. Soc.*, 128, 90 (2006)

The so-called AM1-SRP potential has 32 parameters, obtained through fittings with experimental and simulation data, describes different pathways from a single reactant to three products (Doubleday et al., *J. Am. Chem. Soc.*, 2006).

# The caldera potential energy surface

**Caldera potential:** a shallow potential well with two pairs of symmetry related index-1 saddles associated with entrance/exit channels.

**Index-1 saddle:** a critical point of the potential corresponding to a local minimum in one direction and a local maximum in another.



From Collins, Kramer, Carpenter, Ezra, Wiggins, J. Chem. Phys., 141, 034111 (2014)

# The caldera Hamiltonian system

We consider the **2 degree of freedom Hamiltonian system** (Collins et al., J. Chem. Phys., 2014 - Katsanikas, Wiggins, Int. J. Bifurcat. Chaos, 2018; 2019 - Katsanikas et al., Int. J. Bifurcat. Chaos, 2020; Chem. Phys. Lett., 2020):

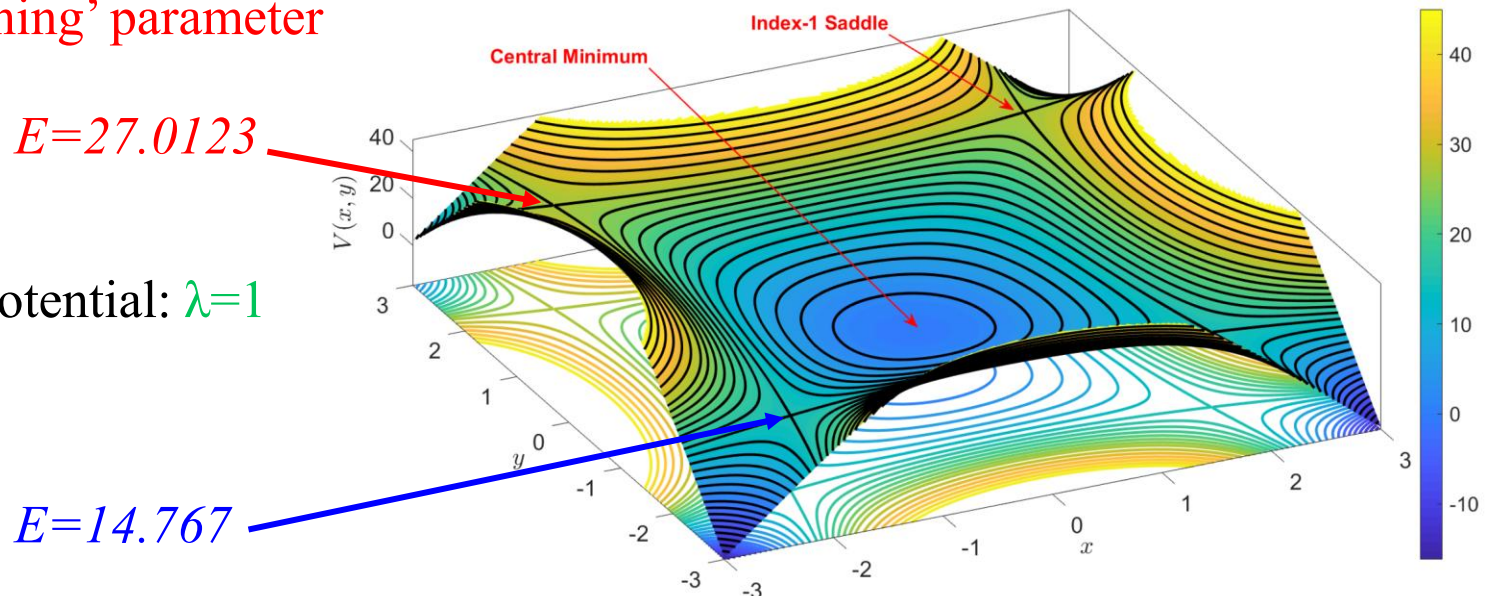
$$H(x, y, p_x, p_y) = \frac{1}{2} (p_x^2 + p_y^2) + V(x, y)$$

where

$$V(x, y) = c_1[(\lambda x)^2 + y^2] + c_2 y - c_3[(\lambda x)^4 + y^4 - 6(\lambda x)^2 y^2],$$

with  $c_1 = 5, c_2 = 3, c_3 = -0.3$ ,  $E = H(x, y, p_x, p_y)$  is the system's energy and  $\lambda$  being a 'stretching' parameter

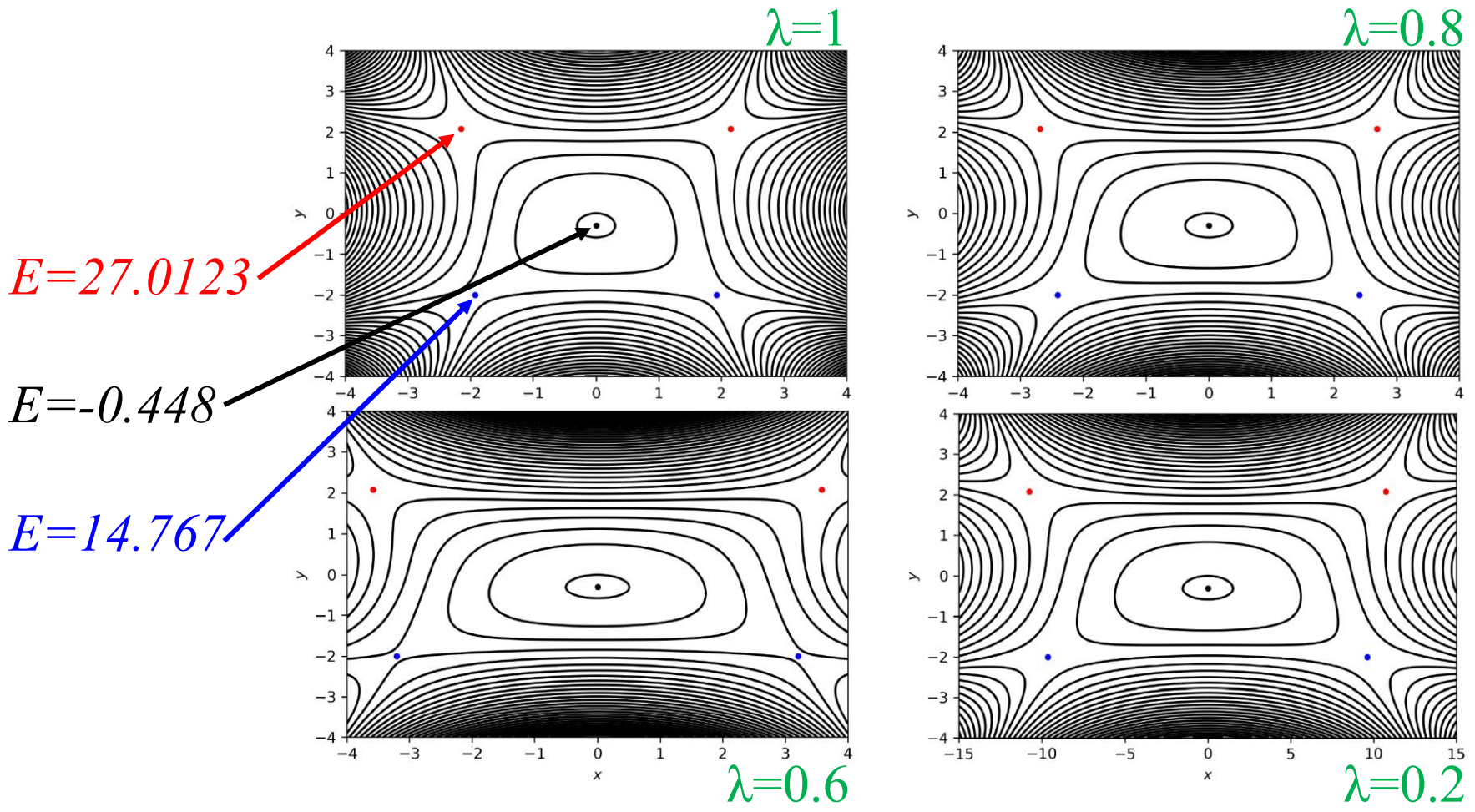
Symmetric potential:  $\lambda=1$



# The caldera Hamiltonian system

$$V(x, y) = c_1[(\lambda x)^2 + y^2] + c_2 y - c_3[(\lambda x)^4 + y^4 - 6(\lambda x)^2 y^2]$$

Stretched potential (typically,  $0 < \lambda < 1$ )



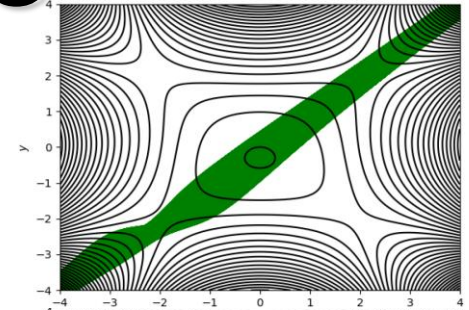
# Dynamical matching

**Dynamical matching:** the momentum direction associated with an incoming orbit initiated at a high energy saddle point, practically determines the outcome of the reaction, i.e. the orbit passes through the diametrically opposing exit channel.

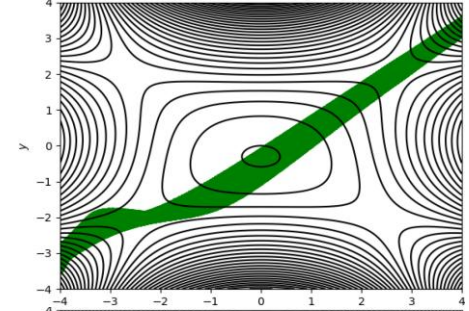
**Critical value** for the breaking of dynamical matching:  $\lambda = 0.778$  (Katsanikas et al., Int. J. Bifurcat. Chaos, 2020)

The **unstable manifolds of the unstable periodic orbits of the upper saddles start interacting** with the **stable manifolds of the central area unstable periodic orbits.**

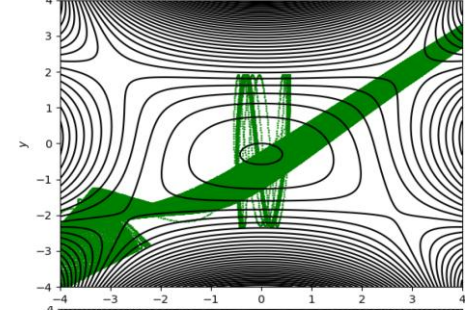
$$\lambda=1$$



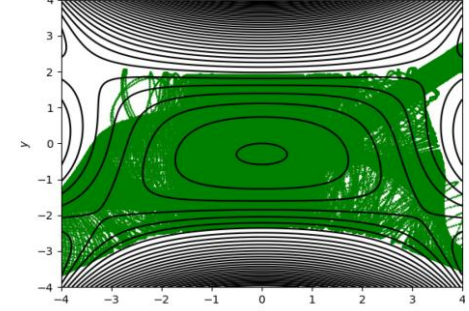
$$\lambda=0.8$$



$$\lambda=0.72$$



$$\lambda=0.6$$



# The origin fate map (OFM)

**Origin fate map (OFM):** We assign to sets of initial conditions a particular combination of indices indicating their origin or start state (through backward integration) and their fate or end state (via forward integration).

Symmetric potential:  $\lambda=1$

Poincaré surface of section (PSS):

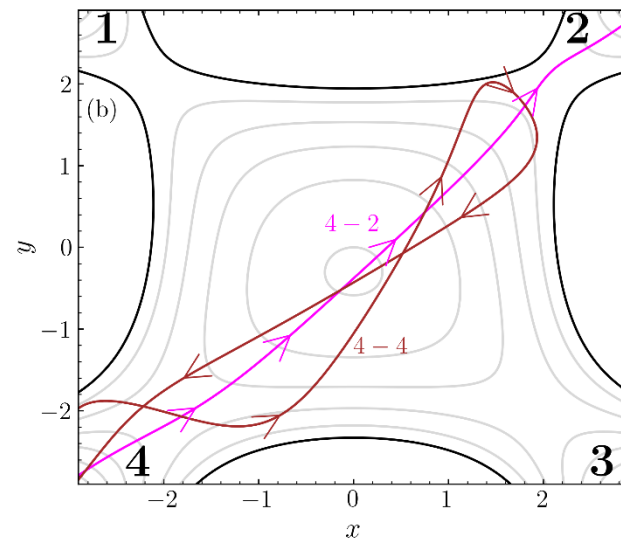
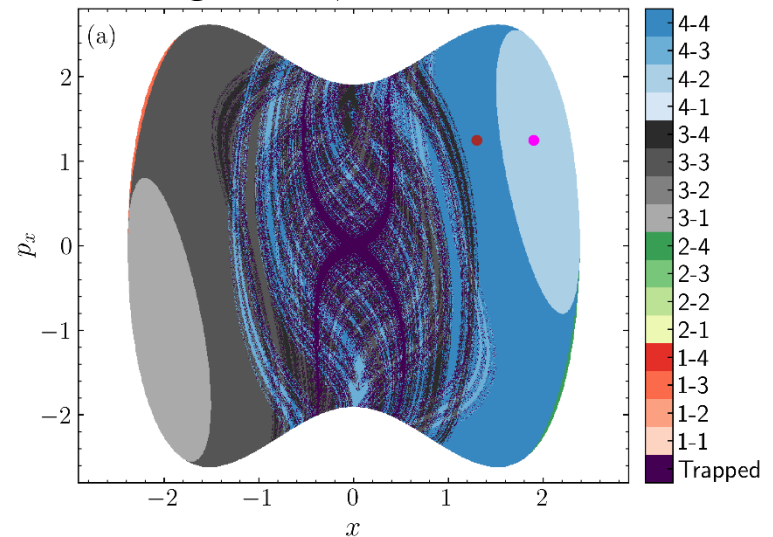
$$y = 1.88409, \quad p_y > 0,$$

$$E = 29.$$

Integration time:  $\tau = 20$  time units.

**Escape condition:**  $|y| > 6$

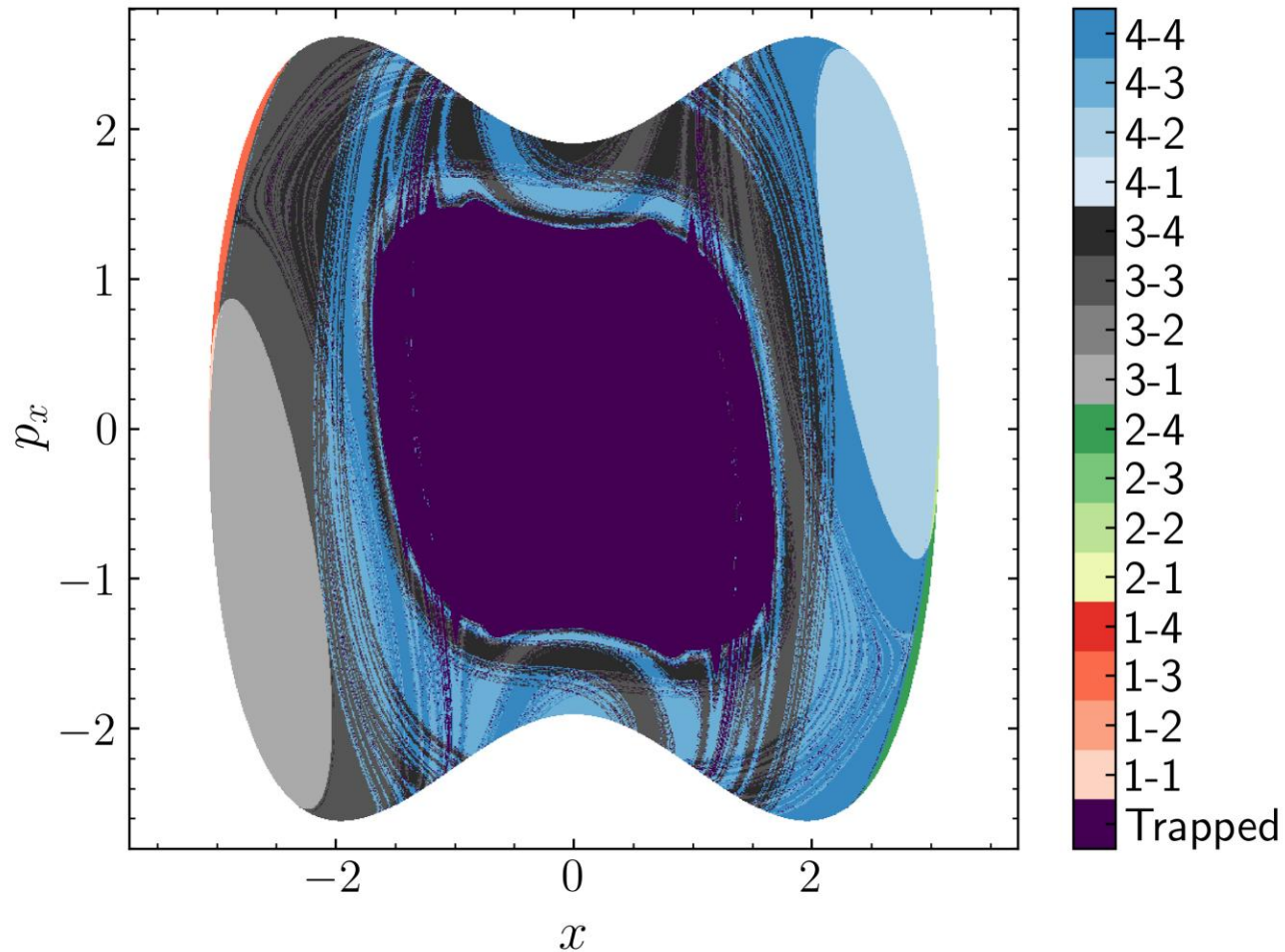
**Trapped:** an orbit does not escape in either the forward or backward integration.



# The origin fate map (OFM)

Stretched potential:  $\lambda=0.778$

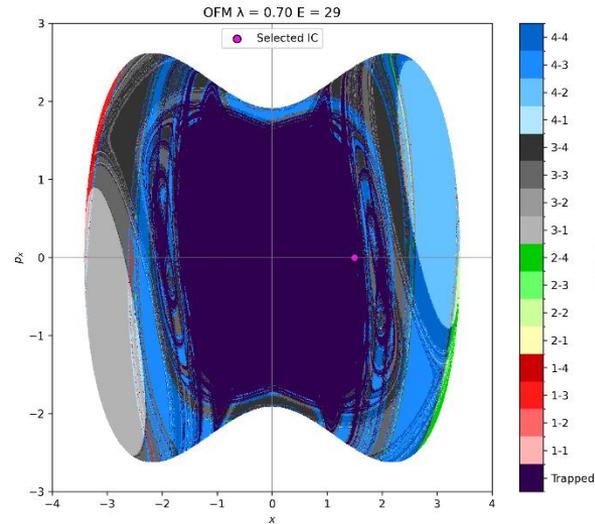
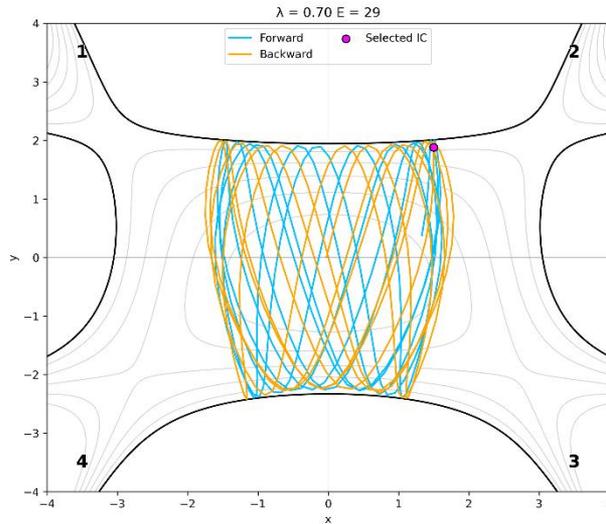
PSS:  $y = 1.88409$ ,  $p_y > 0$ ,  $E = 29$ . Integration time:  $\tau = 20$  time units.



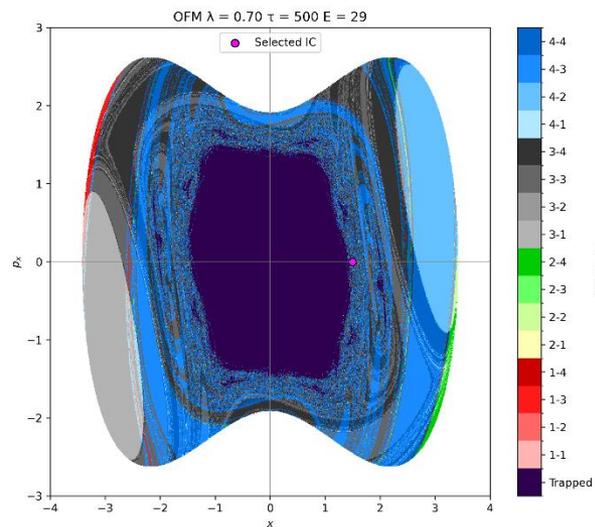
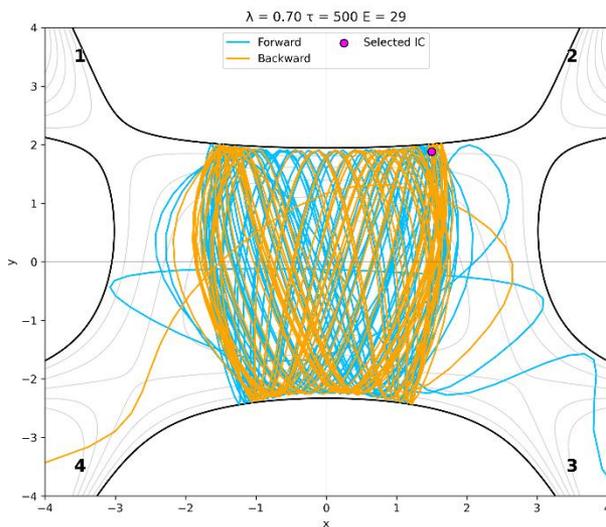
# The origin fate map (OFM)

Stretched potential:  $\lambda=0.7$

PSS:  $y = 1.88409$ ,  $p_y > 0$ ,  $E = 29$ . Selected initial condition:  $x = 1.5$ .



$\tau = 20$

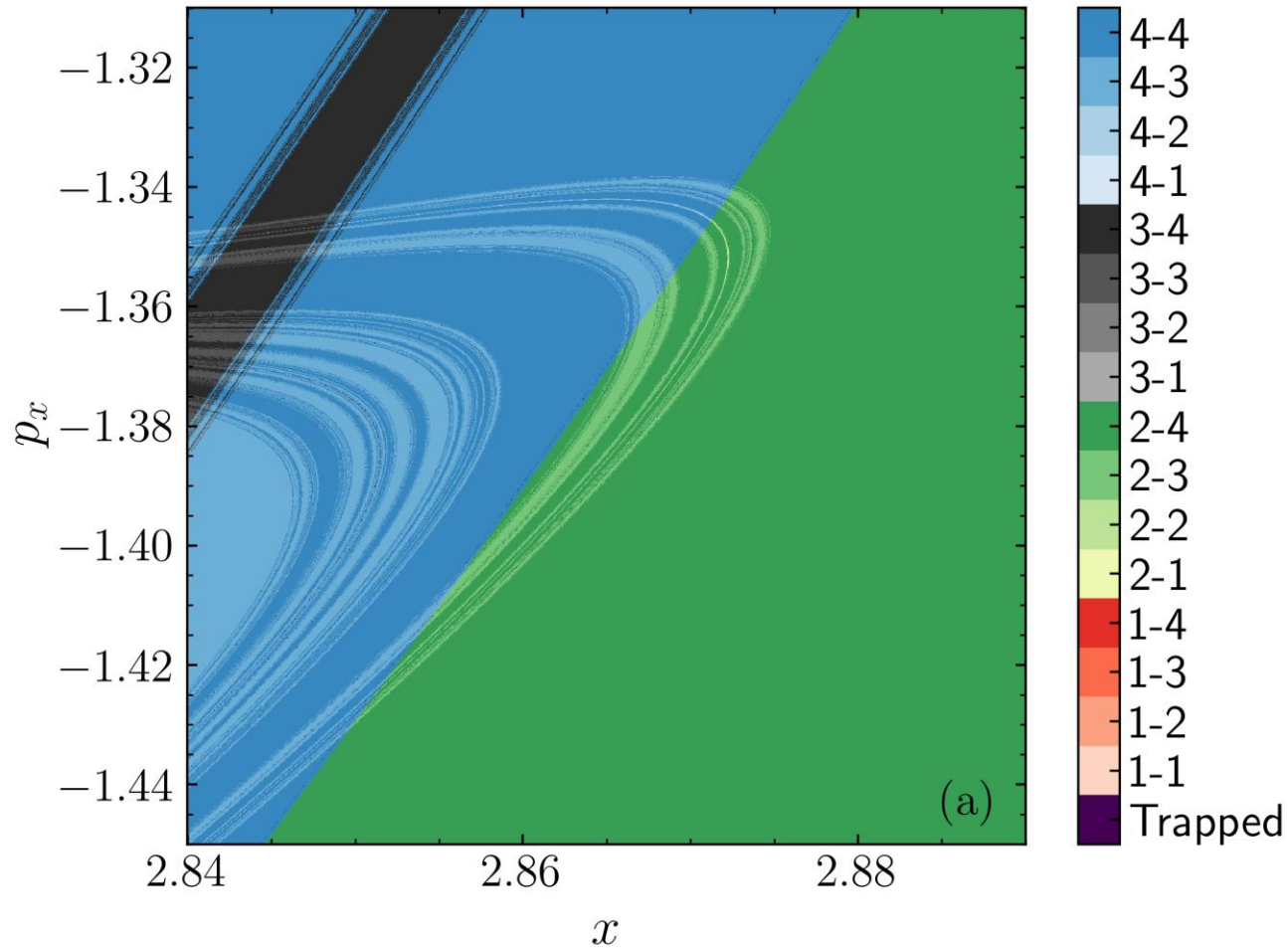


$\tau = 500$

# OFM and manifold dynamics

Stretched potential:  $\lambda=0.778$

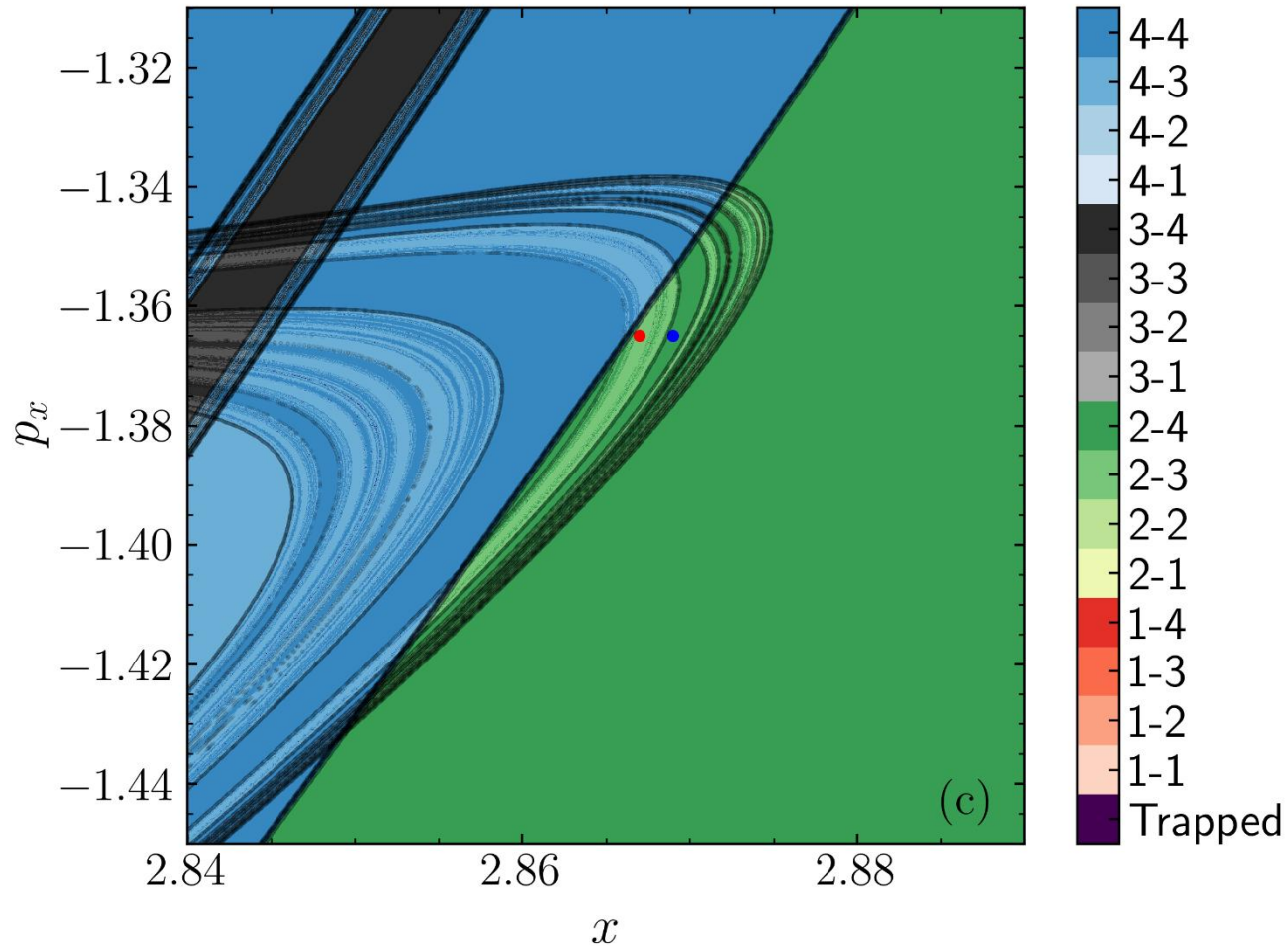
PSS:  $y = 1.88409$ ,  $p_y > 0$ ,  $E = 29$ . Integration time:  $\tau = 20$  time units.



# OFM and manifold dynamics

Stretched potential:  $\lambda=0.778$

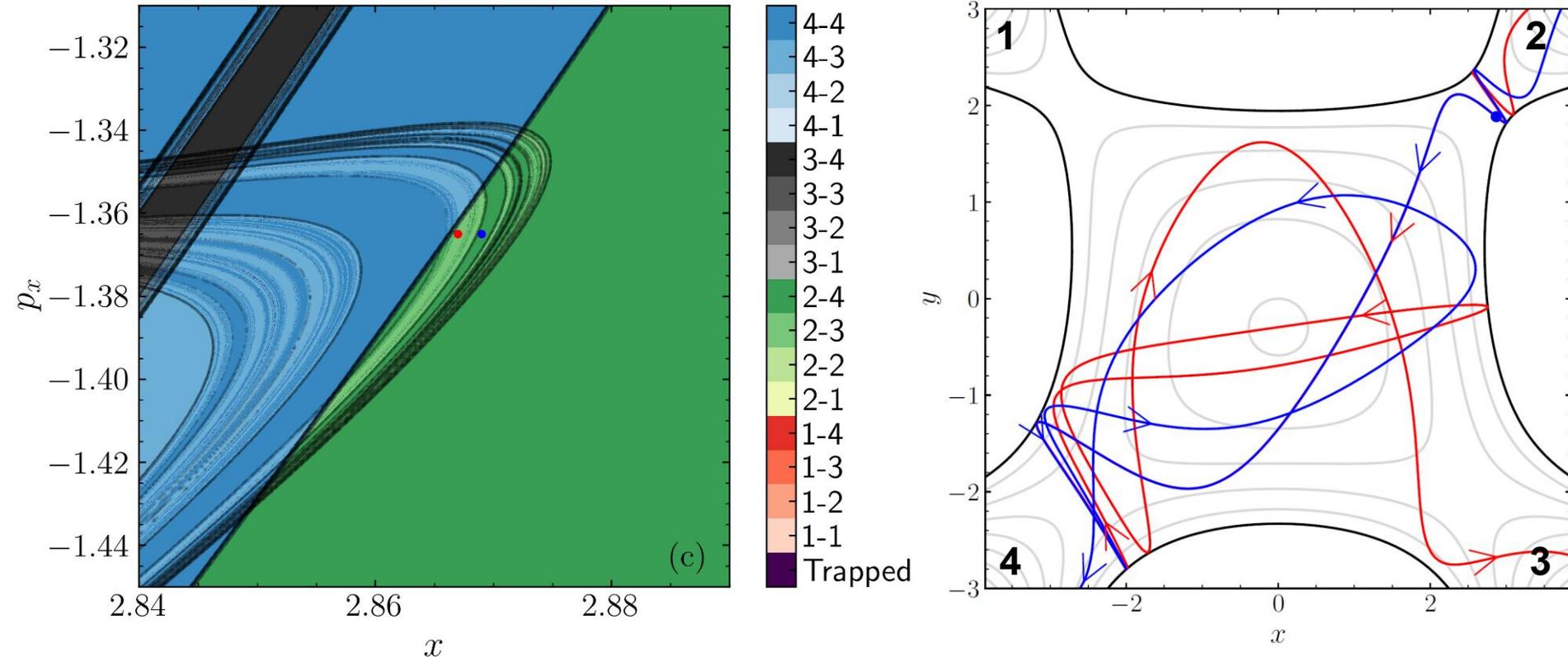
PSS:  $y = 1.88409$ ,  $p_y > 0$ ,  $E = 29$ . Integration time:  $\tau = 20$  time units.



# OFM and manifold dynamics

Stretched potential:  $\lambda=0.778$

PSS:  $y = 1.88409$ ,  $p_y > 0$ ,  $E = 29$ . Integration time:  $\tau = 20$  time units.



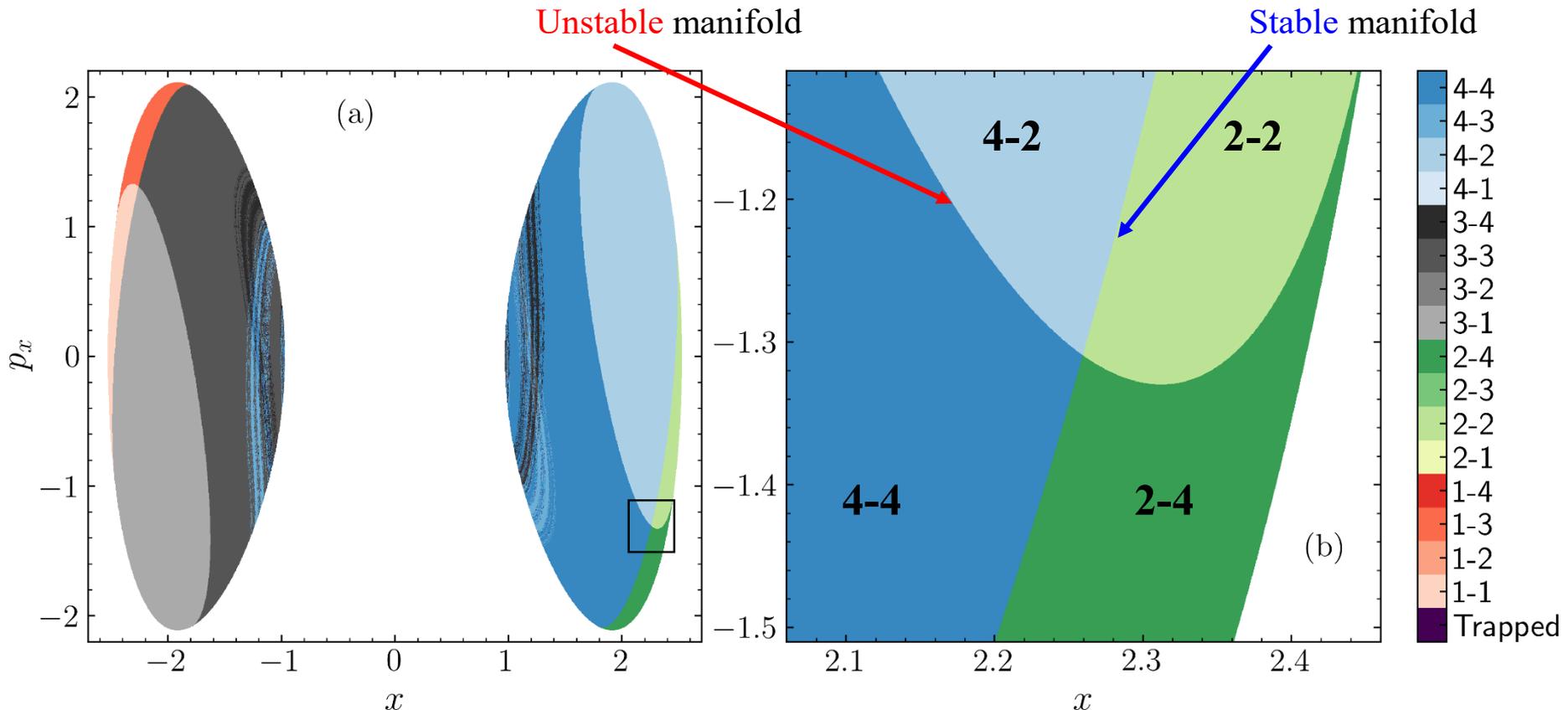
$$(x, y, p_x, p_y) = (2.876, 1.88409, -1.365, 0.86563646)$$

$$(x, y, p_x, p_y) = (2.869, 1.88409, -1.365, 0.85272480)$$

# Locating unstable periodic orbits (UPOs)

UPOs are located at the intersection of stable and unstable manifolds, i.e. at corner points of the OFM.

Change in the origin (fate) index: crossing of a stable (unstable) manifold, which governs backward (forward)-time transport.



Symmetric potential:  $\lambda=1.0$ . PSS:  $y = 2.0$ ,  $p_y > 0$ ,  $E = 29$ ,  $\tau = 20$ .

# Summary I

- ✓ We introduced and successfully implemented computationally efficient ways to **effectively identify chaos** in conservative dynamical systems **from the values of LDs at neighboring initial conditions**.
- ✓ From the distributions of the indices' values we determine appropriate **threshold values**, which allow the characterization of orbits as regular or chaotic.
- ✓ All indices **faced problems** in correctly revealing the nature of some orbits mainly **at the borders of stability islands**.
- ✓ All indices show **overall very good performance**, as their classifications are in accordance with the ones obtained by **the SALI (which is a very efficient and accurate chaos indicator)** at a level of at least 90% agreement.
- ✓ **Advantages:**
  - **Easy to compute** (actually only the forward LDs are needed).
  - **No need to know and to integrate the variational equations.**

# Summary II

- ✓ Origin fate map: coloring initial conditions according to both their past (origin – backward time integration) and their future (fate – forward time integration) evolution.
- ✓ Clear visualization of the system's dynamics and phase space transport along with their evolution in time.
- ✓ Revelation of both stable and unstable manifold behavior.
- ✓ Assist the accurate estimation of the position of unstable periodic orbits.
- ✓ The idea of the OFT is straightforwardly extensible to different open Hamiltonian models with escapes, and to dissipative systems with forward- and backward-time attractors.
- ✓ The technique works for Hamiltonian and non-Hamiltonian systems.
- ✓ The definition of an origin/fate state depends on the properties of the system, and could be an attractor, escape channel, spatially localized region, etc.

# References

- Madrid & Mancho, *Chaos*, 19, 013111 (2009)
- Mendoza & Mancho, *PRL*, 105, 038501 (2010)
- Mancho, Wiggins, Curbelo & Mendoza, *Commun. Nonlin. Sci. Num. Simul.*, 18, 3530 (2013)
- Lopesino, Balibrea, Wiggins & Mancho, *Commun. Nonlin. Sci. Num. Simul.*, 27, 40 (2015)
- Lopesino, Balibrea-Iniesta, García-Garrido, Wiggins & Mancho, *Int. J. Bifurc. Chaos*, 27, 1730001 (2017)
- Agaoglou, Aguilar-Sanjuan, García-Garrido, González-Montoya, Katsanikas, Krajňák, Naik & Wiggins, ‘Lagrangian descriptors: Discovery and quantification of phase space structure and transport’, <https://doi.org/10.5281/zenodo.3958985> (2020)
- Montes, Revuelta & Borondo, *Commun. Nonlin. Sci. Num. Simul.*, 102, 105860 (2021)
- Daquin, Pédenon-Orlanducci, Agaoglou, García-Sánchez & Mancho, *Physica D*, 442, 133520 (2022)
- S., *J. Phys. A*, 34, 10029 (2001)
- S., Antonopoulos, Bountis & Vrahatis, *J. Phys. A*, 37, 6269 (2004)
- S. & Manos, *Lect. Notes Phys.*, 915, 129 (2016)
- Collins, Kramer, Carpenter, Ezra, Wiggins, *J. Chem. Phys.*, 141, 034111 (2014)
- Doubleday, Suhrada, Houk, *J. Am. Chem. Soc.*, 128, 90 (2006)
- Katsanikas, Wiggins, *Int. J. Bifurcat. Chaos*, 28, 1830042 (2018)
- Katsanikas, Wiggins, *Int. J. Bifurcat. Chaos*, 29, 1950057 (2019)
- Katsanikas, García-Garrido, Wiggins, *Int. J. Bifurcat. Chaos*, 30, 2030026 (2020)
- Katsanikas, García-Garrido, Wiggins, *Chem. Phys. Lett.*, 743, 137199 (2020)

Hillebrand, Zimper, Ngapasare, Katsanikas, Wiggins & S.: *Chaos*, 32, 123122 (2022), ‘Quantifying chaos using Lagrangian descriptors’

Zimper, Ngapasare, Hillebrand, Katsanikas, Wiggins & S.: *Physica D*, 453, 133833 (2023), ‘Performance of chaos diagnostics based on Lagrangian descriptors. Application to the 4D standard map’

Hillebrand, Katsanikas, Wiggins & S.: *Phys. Rev. E*, 108, 024211 (2023), ‘Navigating phase space transport with the origin-fate map’